THE PERFORMANCE OF AUTOMATIC ADAPTIVE EDGE-BASED SMOOTHED FINITE

ELEMENT METHOD IN ENGINEERING MECHANICS APPLICATIONS

Mr. Vu Hoang Le

จุฬาลงกรณ์มหาวิทยาลัย

CHULALONGKORN UNIVERSITY

A Thesis Submitted in Partial Fulfillment of the Requirements

for the Degree of Master of Engineering in Civil Engineering

Department of Civil Engineering

Faculty of Engineering

Chulalongkorn University

Academic Year 2019

อิทธิพลของระเบียบวิธี ES-FEM ที่ปรับขนาดชิ้นส่วนอัตโนมัติในการประยุกต์ใช้กลศาสตร์วิศวกรรม

นายวู เหิง ลี

Thesis Title	THE PERFORMANCE OF AUTOMATIC ADAPTIVE EDGE-BASED SMOOTHED FINITE ELEMENT METHOD IN ENGINEERING MECHANICS APPLICATIONS
By	Mr. Vu Hoang Le
Field of Study	Civil Engineering
Thesis Advisor	Assistant Professor SAWEKCHAI TANGARAMVONG, Ph.D.

Accepted by the Faculty of Engineering, Chulalongkorn University in Partial Fulfillment of the Requirement for the Master of Engineering

　　　　　　　　　　　　　　　　　　　　　　　　　　 Dean of the Faculty of Engineering
　　　　(Professor SUPOT TEACHAVORASINSKUN, D.Eng.)

THESIS COMMITTEE

　　　　　　　　　　　　　　　　　　　　　　　　　　 Chairman
　　　　(Professor Teerapong Senjuntichai, D.Eng.)

　　　　　　　　　　　　　　　　　　　　　　　　　　 Thesis Advisor
　　　　(Assistant Professor SAWEKCHAI TANGARAMVONG, Ph.D.)

　　　　　　　　　　　　　　　　　　　　　　　　　　 Examiner
　　　　(Associate Professor Jaroon Rungamornrat, D.Eng.)

　　　　　　　　　　　　　　　　　　　　　　　　　　 Examiner
　　　　(Professor Thaksin Thepchatri, Ph.D.)

　　　　　　　　　　　　　　　　　　　　　　　　　　 External Examiner
　　　　(Assistant Professor Suriyon Prempramote, D.Eng.)

วู เหิง ลี : อิทธิพลของระเบียบวิธี ES-FEM ที่ปรับขนาดชิ้นส่วนอัตโนมัติในการ ประยุกต์ใช้กลศาสตร์วิศวกรรม. (THE PERFORMANCE OF AUTOMATIC ADAPTIVE EDGE-BASED SMOOTHED FINITE ELEMENT METHOD IN ENGINEERING MECHANICS APPLICATIONS) อ.ที่ปรึกษาหลัก : เสวกชัย ตั้งอร่ามวงศ์

-วิทยานิพนธ์เล่มนี้ศึกษาความสามารถของระเบียบวิธี edge-based smoothed finite element หรือ ES-FEM ที่ถูกพัฒนารวมกับกระบวนการแบ่งตัวอัตโนมัติของชิ้นส่วนประกอบ แบบจำลองคอมพิวเตอร์ในการประเมินพฤติกรรมเชิงกลของโครงสร้างภายใต้แรงกระทำในช่วงการ ยืดหยุ่นของวัสดุ ระเบียบวิธี ES-FEM ถูกพัฒนาจากการใช้ค่าเฉลี่ยอิงน้ำหนักของความเครียดที่ เกิดขึ้นตามแนวขอบเขตที่ใช้ร่วมกันระหว่างชิ้นส่วนประกอบแบบจำลองคอมพิวเตอร์ ในขณะที่ ชิ้นส่วนที่มีลักษณะพิเศษประกอบไปด้วยจำนวนจุดห้าจุด ถูกใช้ในการแก้ปัญหาของโครงสร้างที่ ความเค้นภาวะเอกฐาน ชิ้นส่วนที่มีลักษณะพิเศษนี้สามารถนำมาใช้ร่วมกับชิ้นส่วนปรกติแบบสาม จุดได้เป็นอย่างดี โดยการแบ่งตัวอัตโนมัติของแบบจำลองคอมพิวเตอร์ใช้ระเบียบวิธี newest node bisection ร่วมกับสมการประเมินค่าความผิดพลาดของความเค้นแบบ L2-norm error estimator ในการระบุชิ้นส่วนในแบบจำลองคอมพิวเตอร์ที่มีค่าความเบี่ยงเกินกว่าค่าที่ยอมรับได้ และชิ้นส่วนเหล่านั้นจะถูกพิจารณาลดขนาดอัตโนมัติ จากการทดลองแก้ปัญหากลศาสตร์โครงสร้าง จำนวนมาก พบว่าการพัฒนาระเบียบวิธีการวิเคราะห์โครงสร้างที่นำเสนอในวิทยานิพนธ์เล่มนี้ สามารถนำมาใช้ในการสร้างแบบจำลองคอมพิวเตอร์ของโครงสร้างทางวิศวกรรมที่มีรูปร่างซับซ้อน ได้อย่างถูกต้องและมีประสิทธิภาพ

จุฬาลงกรณ์มหาวิทยาลัย

CHULALONGKORN UNIVERSITY

สาขาวิชา วิศวกรรมโยธา   ลายมือชื่อนิสิต ....

ปีการศึกษา 2562   ลายมือชื่อ อ.ที่ปรึกษาหลัก ....

6070497421 : MAJOR CIVIL ENGINEERING

KEYWORD: Edge-Based Smoothed Finite Element Method Automatic Adaptive
             Mesh Algorithm Recovery-Based Error Estimator Newest Vertex
             Bisection Singular Element.
             Vu Hoang Le : THE PERFORMANCE OF AUTOMATIC ADAPTIVE EDGE-BASED
             SMOOTHED FINITE ELEMENT METHOD IN ENGINEERING MECHANICS
             APPLICATIONS. Advisor: Asst. Prof. SAWEKCHAI TANGARAMVONG, Ph.D.

-The thesis investigates the performance of an edge-based smoothed finite element method (ES-FEM) combined with an automatic mesh refinement (AMR) algorithm to provide the solutions of in-plane elastic engineering mechanics applications. The ES-FEM adopts a strain smoothing technique over the edges adjoining the two adjacent triangular-shape meshes, whilst a layer of singular yet compatible five-node elements in addition to standard three-node ES-FEs can be employed to overcome the problems associated with stress singularity.

The proposed framework enables the effective model construction of realistic engineering structures with complex geometry at modest computational resources. The AMR algorithm adopts the newest node bisection scheme that automatically sub-divides the parent critical elements into a suitable number of smaller children members at the longest edge of three-node elements overcoming the hang-node problems. The set of critical members is determined by the L2-norm error estimator functions defining the difference between the computed numerical von Mises stress solutions and recovery stress values. A number of illustrative, including classical benchmarks, examples were successfully processed by the proposed numerical analysis platform. These hence present the efficiency of the developed analysis framework in approximating the accurate elastic responses of

Field of Study: Civil Engineering	Student's Signature ....
Academic Year: 2019	Advisor's Signature ....

ACKNOWLEDGEMENTS

TABLE OF CONTENTS

จุฬาลงกรณ์มหาวิทยาลัย

CHULALONGKORN UNIVERSITY

CHAPTER 1 INTRODUCTION

1.1 Background and Motivation

The analysis and design of engineering structures is to remaining safety with lowest consuming resource. Not only the models with simple 1-D elements such as bar elements or beam elements but also more complicated problems in 2D or 3D models need to be handled in practical design. The numerical method widely used for getting the solutions to such problems is Finite Element Method or FEM contributed by (Olgierd Cecil Zienkiewicz, Taylor, Nithiarasu, & Zhu, 1977). In the finite element model, a three-node triangular mesh is preferred to use than the others owing to its simplicity and easy adaptation on complex boundaries denoted to FEM-T3. Furthermore, adaptive analysis conforms with a triangular mesh that can be modified and regenerated in an automatic manner. The poor accuracy solutions of FEM-T3 models have been shown by adopting a conventional model construction, especially for problems involving stress concentration and/or stress singularities. The linear interpolation function which provides element-wise constant stress or strain fields seems inappropriate in such cases. An infinity stress value at singular points (namely re-entrant corners in the frame, cracking point, positions at discontinuities in applied loads or point loads, etc.) has theoretically proved in the literature. Other mechanics problems contain singular points in the domain such as material discontinuities in composite structures or stress singularities at sharp edges at the interfaces of two frictional bodies (Comninou, 1976). It causes severe discretization errors associated with coarse meshes in the FEM-T3 models. (Lo, 2014) indicated that the rate of convergence in Finite Element Analysis (FEA) slows down with the presence of singularities in the domain.

However, the standard FEMs using isoparametric element formulations have exhibited an "overly-stiff" response leading to poor accurate solutions, especially linear interpolation elements. The objective of the new method is also using the simplest

element which is aforementioned above as the simple, robust, convenient one for adaptive analysis. In order to improve accuracy, a meshfree technique is integrated into the conventional FEM to form the Smoothed Finite Element Method or S-FEM by G. Liu, Dai, and Nguyen (2007). The diversity of 2D S-FEMs, which is edge-, node- and cell-based 2D models, with different properties owing to the strain smoothing technique from (J. S. Chen, Wu, Yoon, & You, 2001). S-FEM models introduce "softening" effects by computing the elemental stiffness matrices associated with smoothing domains or SDs from the shape function values and not its gradients at gauss points on the boundaries of SDs. Instead of taking information of nodes at the vertices inside each triangle element, the S-FEMs spreads out to consider also nodes from surrounding elements to contribute in each smoothed strain field. The S-FEM has recently been widely performed because of its superior properties such as super-convergent stresses, upper bound solutions, volumetric free-locking (G.-R. Liu, 2009), shear locking (H Nguyen-Xuan, Tran, Nguyen-Thoi, & Vu-Do, 2011) (Hung Nguyen-Xuan, Rabczuk, Nguyen-Thanh, Nguyen-Thoi, & Bordas, 2010), and especially is free of mesh quality requirement. Recently, some extensions and enhancements have been done to open and apply S-FEM in solving more sophisticated problems such as static and dynamic problems (Zhang & Liu, 2010), nonlinear analysis (Cui, Liu, Li, Zhang, & Sun, 2009), high-order elements applications (Bordas et al., 2010); contact (Li, Liu, & Zhang, 2011); fracture problems (L Chen, Liu, Nourbakhsh-Nia, & Zeng, 2010) and (Vu-Bac et al., 2013); etc.

Each S-FEM models exhibited various excellent properties due to its inherent "softening" effects compared with the "overly-stiff" property existing in the original FEM model. Many engineering mechanics applications conducted in the framework of the edge-based smoothed finite element method (ES-FEM) owing to its super-accuracy and stability for numerical solutions and simplicity in implementation. ES-FEM model is eminently suitable for a mesh of polygonal elements with arbitrarily n sides particularly the three-node triangle elements denoted to ES-FEM-T3.

For problems with arbitrary order of singular stress field varying on the reentrant angles, e.g. a 2d problems with a re-entrant corner in (Szabó, Szabo, & Babuška, 1991). This singular model work well either weak or strong singularities problems, expressed by the power singular term λ, with $\pi < \phi \leq 2\pi$ under the free-free boundary conditions (BCs) on both angle faces of the re-entrant corner. (Williams, 1952) and (Seweryn & Molski, 1996) had proved the occurrence of elastic stress singularities at angular corners resulting from various BCs rather than only the free-free BC as normally encountered in crack problems. The λ in the term $(\sigma \sim r^{\lambda-1})$ is interpolated from the graph as provided in (Williams, 1952) or computed from the characteristic Equations in (Seweryn & Molski, 1996) depending on the value of vertex angle and the BCs on the two radial edges.

A refinement scheme is usually considered to obtain improved solutions in the next cycles of analysis. The adaptive procedure will result in increasing the accuracy of the numerical methods through appropriately refining the mesh so that better solutions can be achieved with a reasonable computational effort. Adaptive mesh refinement (AMR) algorithm under various procedures of error estimator and refinement can be implemented using the current numerical solution in each step of analysis. The FEM model under adaptive analysis for mesh of triangle elements has been introduced and gained outstanding results (O. Zienkiewicz & Zhu, 1989) (Johnson & Hansbo, 1992). After getting the initial solution, the procedure continues with the aim of finding the regions inside the domain where high errors have been shown and then refines them. A smaller size element obviously better captures the exact solution especially in problems with stress singularity.

(Nourbakhshnia & Liu, 2011) solved crack propagation problem by adapting the mesh with the Delaunay triangulation procedure and the Laplacian smoothing technique instead of computing error indicators. The error estimating area, however, is essential in the adaptive algorithm for selecting an appropriate group of elements to be refined every iteration. Over the past decades, many significant developments in the area of

error estimation and mesh optimization have been achieved for FEA. (Babuška & Rheinboldt, 1978) used the deviations from the equilibrium equations and the inter-element jump of strain or stress over element boundaries for estimating the numerical error. In addition, an error estimator scheme which use the first-derivative recovery technique introduced by (Olgierd C Zienkiewicz & Zhu, 1987). A recovery stress (or strain) field will be constructed which is demonstrated to be more accurate than the above interelement discontinuous stress field. (Ainsworth, Zhu, Craig, & Zienkiewicz, 1989) has mathematically analyzed the rate of convergence of the so-called posterior error estimator. It then was widely used for adaptive analysis in various FEM models in (O. Zienkiewicz & Zhu, 1989). (Jayaswal & Grosse, 1993) showed that simplicity and low computing resource are obtained in case of performing recovery-based error estimator based upon a scalar stress function than a stress tensor function. Therefore, a simple error indicator with recovery technique generated from von Mises stress function in L2-norm is adopted in the present work both in FEM-T3 and ES-FEM-T3 framework.

In the FEM-T3, the stress (or strain) is continuous in each triangle element, while the smoothed stress (or strain) is constant and discontinuous along the boundaries of SDs inside triangular elements. Several adaptive analysis applications in S-FEMs, however, conducted by (Nguyen-Thoi, Liu, Nguyen-Xuan, & Nguyen-Tran, 2011) or (Hung Nguyen-Xuan, Liu, Bordas, Natarajan, & Rabczuk, 2013) did not specifically provide formulations for estimating these error indicators. In this work, simple and exact formulations for recovery-based error estimator of von Mises stresses in L2-norm is established in ES-FEM-T3/singular ES-FEM-T3 models. Moreover, it is straightforward and easy-to-programming in a vector-based language.

In order to enhance the efficiency of the proposed models, vectorization for programming within a MATLAB environment is used which reduces the required computational runtime and storage especially in large-scale or complicated mechanics problems. The process of revising the loop- and scalar-based operations into matrix- and vector-oriented operations is known as vectorization. Recently, some efforts have

been made for the S-FEMs to be simplest and most general as possible (Li, Li, & Liu, 2014) (Niu, Liu, & Yue, 2018). Some ideas of using matrix-based operations were first introduced by (Getreuer, 2006) in MATLAB programming. In this work, we will apply vectorization into some parts of the adaptive procedure for the three-node ES-FEM and singular ES-FEM to further augment the robustness and the efficiency of the proposed adaptive scheme.

The applications of node-based smoothed finite element method or NS-FEM using a similar recovery-based error function were described in (Nguyen-Thoi et al., 2011). where it demonstrated clearly the good convergence capability and upper-bound strain energy solutions over iterative mesh reconstruction processes. The singular ES-FEM (Hung Nguyen-Xuan et al., 2013) adopted a recovery-based error indicator in an energy norm to predict accurately singular stress field under the free-free boundary condition on both angle faces around the re-entrant corners. The proposed adaptive mesh implementation adopts the vertex bisection algorithm with recovery-based error estimators that automatically decides the critical remeshing elements based on the discrepancy between numerical solutions and the so-called recovery solution. The specific error indicator with recovery technique in L2-norm is adopted within the framework of FEM-T3 and ES-FEM-T3 for analysing engineering structures. The similar application into singular ES-FEM-T3 for the problems having angular corners under several BCs, such as free-free, free-simply supported and clamped-free, using the proposed mesh adaptation is also investigated. The variety of BCs occur in several numerical models that represent only a part of the practical structure because of symmetry. Some numerical examples subjected to the difficulties associated with elastic stress singularity and discontinuity are given to illustrate applications of the developed analysis scheme. It describes a significant reduction of computing resources as compared to standard model construction procedures. Moreover, the proposed mesh adaptation can efficiently converge the stress response results over the local areas of structures considered.

1.2 Research Objective

From the aforementioned contents, the main research objectives in this work as follows:

(1) Analyzing the plane strain and plane stress mechanics problems in the framework of FEM-T3, FEM-Q4 and ES-FEM-T3 under the uniform model construction. The results from several numerical examples are expected to provide a more efficient and robust elastic analysis scheme both degrees of freedoms (DOFs) and CPU time of the ES-FEM-T3 model.

(2) A simple yet effective recovery-based error function of von Mises stresses in L2-norm adopted directly to the automatic AMR scheme is applied into an ES-FEM-T3 framework. The proposed analysis work provides the elastic responses of engineering mechanics problems associated with physically instabilizing stress singularity and discontinuity field. Some numerical examples subjected to the difficulties associated with elastic stress singularity and discontinuity are provided to illustrate efficiency and robustness of the proposed analysis framework

(3) The proposed adaptive mesh implementation is adopted (in a similar fashion to the conventional FEM) for the singular ES-FEM-T3 model with a layer of singular five-node elements around the crack point that can produce the stress singularities of arbitrary order. The examples having angular corners under different BCs, namely, free-free, simply supported-simply supported, and clamped-free on the two angle faces are tested to validate the super-accuracy and the fast-convergence propertied of present method.

(4) MATLAB built-in functions and vectorization will be applied in our tool in order to optimize the efficiency of consuming computational resources such as runtime and storage. The superiority in computing resources is verified in some log-scale figures.

1.3 Scope of Research

From the mentioned above research objectives, the scope of research in this work is listed below:

(1) Solving plane strain and plane stress mechanics problems in linear elastic materials

(2) The simplest three-node triangle element for the general case and the singular five-node triangle element for the particular case of stress singularity are properly applied in the proposed analysis framework

(3) Applying a strain smoothing technique on the standard FEM-T3 associated with edges of triangular mesh to establish the ES-/singular ES-FEM-T3.

(4) Applying Adaptive Mesh Refinement (AMR) technique under the proposed analysis framework to obtain the optimal mesh for engineering mechanics problems involving stress concentration and singularities

(5) In programming, the extension of the elementwise array operations into the matrix-wise array operations or the matrix-array operations is conducted. It is performed in the sense of eliminating as many as possible for-loops by using matrix-array operations and built-in functions within a MATLAB environment.

1.4 Methodology and Research Procedure

In this work, we investigate the performance of a novel automatic adaptive ES-FEM-T3 for general problems and automatic adaptive singular ES-FEM-T3 for problems with stress singularities resulting from various BCs in terms of high performance, e.g. accuracy, simplicity, and less computational consumption, to provide the solutions of two-dimensional practical engineering mechanics problems.

Following this purpose of the study, several tasks for implementation are listed below: Firstly, the numerical method ES-FEM-T3 are tested to prove a more efficient and robust elastic analysis scheme as compared with the standard FEM using isoparametric elements.

Sencondly, a simple yet effective recovery-based error function of von Mises stresses adopted directly to the automatic AMR scheme within the framework of ES-/singular ES-FEM-T3. The propose analysis scheme provides the elastic responses of engineering mechanics problems associated with physically instabilizing stress singularity. The results from several benchmark examples showed that the proposed mesh adaptation

can efficiently converge the stress response results over the local areas of structures considered.

Finally, vectorization language and several advanced built-in functions in MATLAB will be employed for numerical methods under the proposed mesh adaptation to reduce the requirement of computational resources. The results from several examples will validate the performance of the present analysis model in terms of simplicity, accuracy and less consumption of computational resources.

CHAPTER 2 LITERATURE REVIEW

2.1 Problem Description.

2.1.1 General.

Fig. 2.1 represents a 2D linear-elastic solid body of Ω with the boundary Γ divided into two parts, Dirichlet conditions denoted by Γ_D where displacements u are presented and Neumann conditions denoted by Γ_N where tractions t are pressented. The domain is subjected to a body force and b and are classified into two cases of corner with BCs on two angle faces, namly free-free Fig. 2.1a) and clamped-free Fig. 2.1b) such that $\Gamma = \Gamma_D \cup \Gamma_N, \Gamma_D \cap \Gamma_N = \varnothing$.
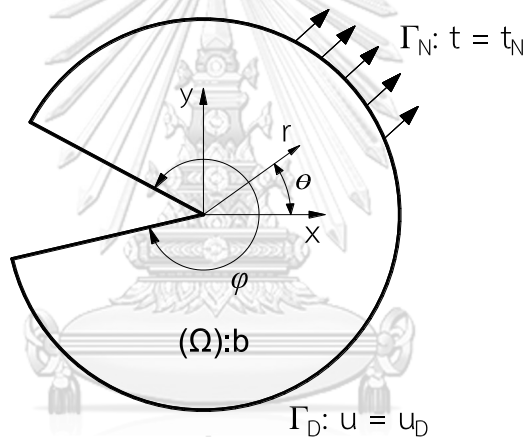
a) Sharp corner with vertex angle φ under the free-free BC
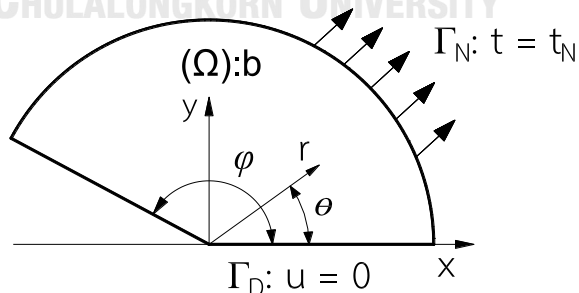
b) Sharp corner with vertex angle φ under the clamped-free BC

Figure 2.1 Two-dimensional domains resulting in an arbitrary order of singular stress field varying in vertex angle φ and BCs of the two angle faces.

2.1.2 Governing Equations.

According to the linear elastic theory, the 2D time-independent mechanic's problems can be described through the solution of Boundary Value Problem (BVP) as follows:

$$\sigma_{ij} + b_i = 0; \forall x \in \Omega \tag{2.1}$$

$$\sigma_{ij} = C_{ijkl}\varepsilon_{kl}; \forall x \in \Omega \tag{2.2}$$

$$\varepsilon_{ij} = \frac{1}{2}\left(u_{i,j} + u_{j,i}\right); \forall x \in \Omega \tag{2.3}$$

And Boundary Conditions:

- Prescribed displacement: $\quad u_i = u_D(x); \forall x \in \Gamma_D \tag{2.4}$

- Prescribed traction: $\quad \sigma_{ij}n_j = t_N(x); \forall x \in \Gamma_N \tag{2.5}$

on angle faces:

Case a: $\quad \begin{cases} u_\theta = \tau_{r\theta} = 0 & for \ \theta = 0 \\ \sigma_\theta = \tau_{r\theta} = 0 & for \ \theta = \varphi \end{cases} \tag{2.6a}$

Case b: $\quad \begin{cases} u_r = u_\theta = 0 & for \ \theta = 0 \\ \sigma_\theta = \tau_{r\theta} = 0 & for \ \theta = \varphi \end{cases} \tag{2.6b}$

where C_{ijkl} = the elastic tensor

In case of using isotropic linear material, C_{ijkl} is deduced by Eq. (2.7) or Eq. (2.8)

Plane stress: $\quad \begin{Bmatrix} \sigma_{xx} \\ \sigma_{yy} \\ \tau_{xy} \end{Bmatrix} = \frac{E}{(1-v^2)} \begin{bmatrix} 1 & v & 0 \\ v & 1 & 0 \\ 0 & 0 & \frac{1-v}{2} \end{bmatrix} \begin{Bmatrix} \varepsilon_{xx} \\ \varepsilon_{yy} \\ \gamma_{xy} \end{Bmatrix} \tag{2.7}$

Plane strain: $\quad \begin{Bmatrix} \sigma_{xx} \\ \sigma_{yy} \\ \tau_{xy} \end{Bmatrix} = \frac{E}{(1+v)(1-2v)} \begin{bmatrix} 1-v & v & 0 \\ v & 1-v & 0 \\ 0 & 0 & \frac{1-2v}{2} \end{bmatrix} \begin{Bmatrix} \varepsilon_{xx} \\ \varepsilon_{yy} \\ \gamma_{xy} \end{Bmatrix} \tag{2.8}$

2.1.3 Singularity Problems.

As already studied in the work of (Williams, 1952) or (Seweryn & Molski, 1996) that the stress around the corner of such problems in Fig. 2.1 taking the form of $\sigma \sim r^{\lambda-1}$, where λ depends on vertex angle and BCs of the two angle faces and is interpolated from

the graph as provided in (Williams, 1952) or computed from the characteristic equations in (Seweryn & Molski, 1996) as follows:

Case a:
$$\lambda \sin \varphi + \sin \lambda \varphi = 0 \qquad (2.9)$$

Case b:
$$\lambda^2 \sin^2 \varphi + (3 - 4v)\sin^2 \lambda\varphi - \frac{\left[(3 - 4v) + 1\right]^2}{4} = 0 \qquad (2.10)$$

For example, if $\varphi = 360^0$ we obtain a solution of $\lambda = 1/2$ corresponding to a crack in the domain.

Engineering structures in practical design that have singular point such as a re-entrant corner in the frame, cracking point, point loads resulting stress singularity (as in Figs. 2.2a, b and c) and discontinuities in applied loads or materials as in Fig. 2.2d), etc. More advanced mechanics problems like material discontinuities in the composite elements or a sharp edge at the interface between two bodies with friction (Comninou, 1976) own the stress singularity or discontinuity. In the area surrounding singular point, the sharp change in the stress field, which causes serious discretization errors using coarse mesh, can be seen clearly in Finite Element Analysis (FEA).
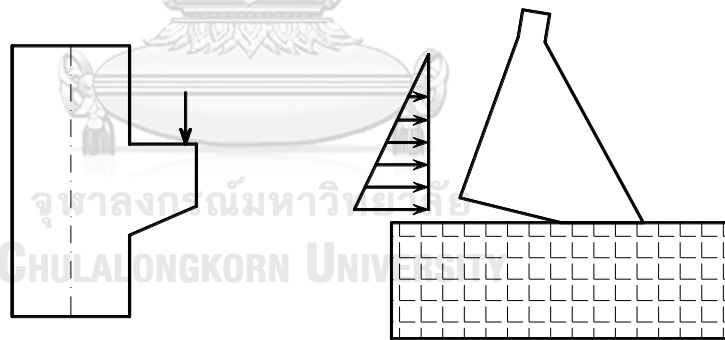
a) Concrete-corbel column with point load b) Concrete dam with interface crack
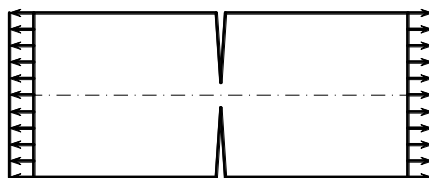
c) Double-edge notched plate   d) Prandtl's punch
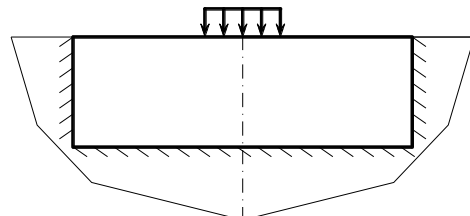
Figure 2.2 Typical structures with singularity point in the domainFinite Element Methods.

2.2 Finite Element Method

2.2.1 Background.

Solving above Partial Differential Equations (PDEs) becomes impossible in case of dealing with complicated problems in geometry, loading conditions, or material properties, etc. The most famous numerical method applied to find the solution to such problems in engineering and mathematical physics is FEM mainly contributed by (Olgierd Cecil Zienkiewicz et al., 1977). FEM gives approximate values of the unknown variables at points of the discrete model. Instead of analytically solving PDE for the whole domain, FEM discretizes a problem into smaller domains so-called elements. Then, the characteristic equations representing these elements are added together into a global system of discrete equations for the entire domain. Recent development of computer science has boosted this method to become more efficient because of its total dependency.

Using finite element modeling, a triangular mesh is usually chosen than the quadrilateral mesh because of its simplicity and easy adaption on the complex boundary.

2.2.2 Isoparametric Three-node Triangular Element.

2.2.2.1 Displacement Interpolation.

In the model of three-node triangle elements, stress and strain fields in each element is piece-wise constant since the interpolation functions are independently linear along each direction.
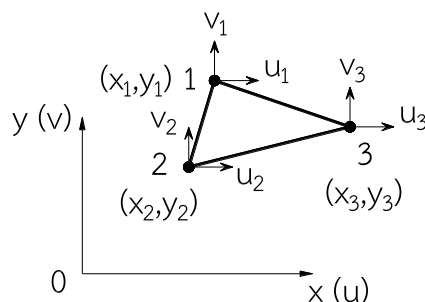
Figure 2.3 Cartesian coordinate system for constant strain elements

+ Two degrees of freedoms or DOF per node are displacements in x- and y- directions. Hence there are six degrees of freedoms per element.

The displacement field is interpolated through shape functions within an element.

$$\tilde{u} = N_i(x,y)\tilde{d}_i$$

Or: $\tilde{u} = \begin{Bmatrix} u(x,y) \\ v(x,y) \end{Bmatrix} = \begin{bmatrix} N_1 & 0 & N_2 & 0 & N_3 & 0 \\ 0 & N_1 & 0 & N_2 & 0 & N_3 \end{bmatrix} \{ u_1 \quad v_1 \quad u_2 \quad v_2 \quad u_3 \quad v_3 \}^T$ (2.11)

where $\tilde{d}_i$ contains nodal displacements.

N_i(x,y) contains shape functions corresponding to the i-th node in the element with the formulation reads

$$\begin{cases} N_1 = \dfrac{m_1 + n_1 + p_1 y}{2A} \\ N_2 = \dfrac{m_2 + n_2 + p_2 y}{2A} \\ N_3 = \dfrac{m_3 + n_3 + p_3 y}{2A} \end{cases}$$ (2.12)

where A is the elemental area, equals to $\dfrac{1}{2}\det\begin{bmatrix} 1 & x_1 & y_1 \\ 1 & x_2 & y_2 \\ 1 & x_3 & y_3 \end{bmatrix}$ (2.13)

and $\begin{cases} m_1 = x_2 y_3 - x_3 y_2 & n_1 = y_2 - y_3 & p_1 = x_3 - x_2 \\ m_2 = x_3 y_1 - x_1 y_3 & n_2 = y_3 - y_1 & p_2 = x_1 - x_3 \\ m_3 = x_1 y_2 - x_2 y_1 & n_3 = y_1 - y_2 & p_3 = x_2 - x_1 \end{cases}$ (2.14)

2.2.2.2 Properties of Shape Functions and Strain-Displacement Matrix
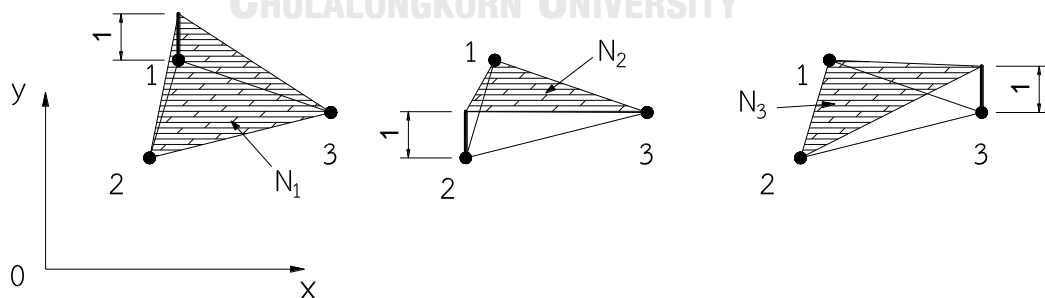
Figure 2.4 Shape functions for three-node triangle element

+ At every point inside the domain: $\begin{cases} N_i = 1 & j = i \\ N_i = 0 & j \neq i \end{cases}$ (2.15)

and $\sum_{i=1}^{3} N_i = 1 ; \quad \sum_{i=1}^{3} N_i x_i = x ; \quad \sum_{i=1}^{3} N_i y_i = y$ (2.16)

+ In 2D triangular mesh:
$$\int_{\Omega_I} N_i N_j \, dx = \begin{cases} A_I/6 & i=j, \\ A_I/12 & i \neq j. \end{cases}$$
(2.17)

Substitute the displacement approximation Eq. (2.11) into the strain-displacement relation Eq. (2.3), then

$$\tilde{\varepsilon} = \begin{Bmatrix} \varepsilon_x \\ \varepsilon_y \\ \varepsilon_{xy} \end{Bmatrix} = \begin{bmatrix} 1 & 0 & 0 & 0 \\ 0 & 0 & 0 & 1 \\ 0 & 1 & 1 & 0 \end{bmatrix} \begin{Bmatrix} \dfrac{\delta u}{\delta x} & \dfrac{\delta u}{\delta y} & \dfrac{\delta v}{\delta x} & \dfrac{\delta v}{\delta y} \end{Bmatrix}^T = \tilde{B}\tilde{d}$$
(2.18)

where $\tilde{B} = \begin{bmatrix} \dfrac{\delta N_1(x,y)}{\delta x} & 0 & \dfrac{\delta N_2(x,y)}{\delta x} & 0 & \dfrac{\delta N_3(x,y)}{\delta x} & 0 \\ 0 & \dfrac{\delta N_1(x,y)}{\delta y} & 0 & \dfrac{\delta N_2(x,y)}{\delta y} & 0 & \dfrac{\delta N_3(x,y)}{\delta y} \\ \dfrac{\delta N_1(x,y)}{\delta y} & \dfrac{\delta N_1(x,y)}{\delta x} & \dfrac{\delta N_2(x,y)}{\delta y} & \dfrac{\delta N_2(x,y)}{\delta x} & \dfrac{\delta N_3(x,y)}{\delta y} & \dfrac{\delta N_3(x,y)}{\delta x} \end{bmatrix}$

or
$$\tilde{B} = \frac{1}{2A} \begin{bmatrix} n_1 & 0 & n_2 & 0 & n_3 & 0 \\ 0 & p_1 & 0 & p_2 & 0 & p_3 \\ p_1 & n_1 & p_2 & n_2 & p_3 & n_3 \end{bmatrix}$$
(2.19)

with n_i (i= 1,2,3); p_i (i= 1,2,3) in the Eq. (2.14).

2.2.2.3 Global Stiffness Matrix and Nodal Load Vector

The global stiffness matrix then reads:
$$\tilde{K} = \sum_{N_e} \tilde{K}^e = \sum_{N_e} \int_{\Omega^e} \left(\tilde{B}^e\right)^T D\left(\tilde{B}^e\right) d\Omega^e = \sum_{N_e} \left(\tilde{B}^e\right)^T D\left(\tilde{B}^e\right) A^e t$$
(2.20)

The nodal load vector:
$$\tilde{f}^e = \sum_{N_e} \int_{\Omega^e} N^T b^e d\Omega + \sum_{N_e} \int_{\Gamma_N^e} N^T t_N^e d\Gamma_N^e + \sum_{i=1}^{N_{node}} p_i$$
(2.21)

where $\tilde{K}^e$ is the e-th elemental stiffness matrix, t is the element thickness, N_e; N_{node} represent the number of element and node, respectively, in the domain.

For the Von Mises stress: this stress is applied to formulate the von Mises yield criterion indicating the yielding state of materials in 2-D and 3-D stress analyses. It can be computed from the Cauchy stress tensor through the general following formulation.

$$\sigma_{von} = \frac{1}{\sqrt{2}} \sqrt{\left(\sigma_{xx} - \sigma_{yy}\right)^2 + \left(\sigma_{yy} - \sigma_{zz}\right)^2 + \left(\sigma_{zz} - \sigma_{xx}\right)^2 + 3(\sigma_{xy}^2 + \sigma_{xy}^2 + \sigma_{xy}^2)}$$
(2.22)

For plane stress:
$$\sigma_{von} = \sqrt{\frac{3}{4}\left(\sigma_{xx}-\sigma_{yy}\right)^2 + 3\sigma_{xy}^2} \qquad (2.23)$$

For plane strain:
$$\sigma_{von} = \sqrt{\left(\sigma_{xx}-\sigma_{yy}\right)^2 + \sigma_{xx}\sigma_{yy} + 3\sigma_{xy}^2} \qquad (2.24)$$

Because of the constant properties of stress components in triangle elements (FEM) or smoothing domains (ES-FEM), the von Mises stress functions is a scalar values which is piecewise constant inside triangles or smoothing domains, respectively.

2.2.3 Isoparametric Four-node Quadrilateral Element.

2.2.3.1 Shape Functions.
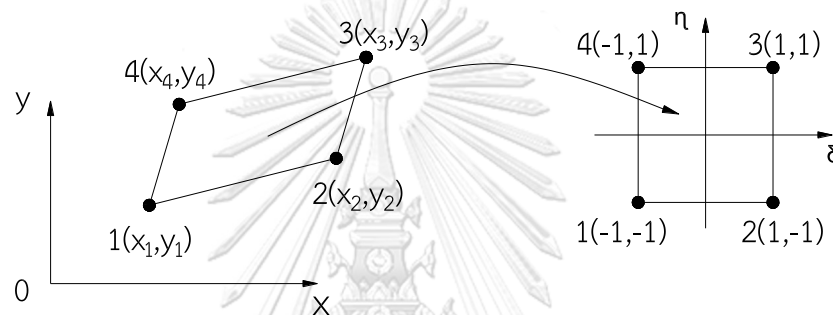
a) Cartesian coordinate system for an arbitrary quadrilateral element;

b) A equivalent square element for natural coordinates.

Figure 2.5 Mapping physical coordinates system into natural coordinates system

The shape functions in the natural coordinate system then reads

$$N_1(\xi,\eta) = \frac{1}{4}(1-\xi)(1-\eta), \quad N_2(\xi,\eta) = \frac{1}{4}(1+\xi)(1-\eta),$$
$$N_3(\xi,\eta) = \frac{1}{4}(1+\xi)(1+\eta), \quad N_4(\xi,\eta) = \frac{1}{4}(1-\xi)(1+\eta). \qquad (2.25)$$

2.2.3.2 Strain-Displacement Matrix.

The transformation The derivatives of the shape functions are transformed from *Oxy* coordinate system to $0\xi\eta$ coordinate system, respectively.

$$\begin{bmatrix} \delta N_j / \delta x \\ \delta N_j / \delta y \end{bmatrix} = J^{-1} \begin{bmatrix} \delta N_j / \delta \xi \\ \delta N_j / \delta \eta \end{bmatrix} \qquad (2.26)$$

where $J = \begin{bmatrix} \delta x / \delta \xi & \delta y / \delta \xi \\ \delta x / \delta \eta & \delta y / \delta \eta \end{bmatrix} \qquad (2.27)$

After substituting into Eq. (2.15), the strain-displacement matrix becomes:

$$\left[\tilde{B}\right]_{3\times 8} = \begin{bmatrix} 1 & 0 & 0 & 0 \\ 0 & 0 & 0 & 1 \\ 0 & 1 & 1 & 0 \end{bmatrix} \left[\Gamma\right]_{4\times 4} \left[N_{,(\xi,\eta)}\right]_{4\times 8} \left\{u_1 \quad v_1 \quad u_2 \quad v_2 \quad u_3 \quad v_3 \quad u_4 \quad v_4\right\}^T \quad (2.28)$$

where $\left[\Gamma\right]_{4\times 4} = \begin{bmatrix} \left[T\right]_{2\times 2} & \left[0\right] \\ \left[0\right] & \left[T\right]_{2\times 2} \end{bmatrix}$ with $\left[T\right]_{2\times 2} = J^{-1} = \dfrac{1}{\det(J)}\begin{bmatrix} J_{22} & -J_{12} \\ -J_{21} & J_{11} \end{bmatrix}$ (2.29)

and $\left[N_{,(\xi,\eta)}\right]_{4\times 8} = \begin{bmatrix} N_{1,\xi} & 0 & N_{2,\xi} & 0 & N_{3,\xi} & 0 & N_{4,\xi} & 0 \\ N_{1,\eta} & 0 & N_{2,\eta} & 0 & N_{3,\eta} & 0 & N_{4,\eta} & 0 \\ 0 & N_{1,\xi} & 0 & N_{2,\xi} & 0 & N_{3,\xi} & 0 & N_{4,\xi} \\ 0 & N_{1,\eta} & 0 & N_{2,\eta} & 0 & N_{3,\eta} & 0 & N_{4,\eta} \end{bmatrix}$ (2.30)

Note: comma ',' represents for the partial derivative.

2.2.3.3 Global Stiffness Matrix and Nodal Load Vector.

The global stiffness matrix reads

$$\tilde{K} = \sum_{N_e} \tilde{K}^e = \sum_{N_e} \int_{-1}^{1}\int_{-1}^{1} \left[\tilde{B}\right]^T D\left[\tilde{B}\right] \det\left(\left[J\right]\right) t\, d\xi\, d\eta \quad (2.31)$$

In order to evaluate the integration in Eq. (2.31), people often use Gauss Integration rules to select some sample points inside each element. The load vector is computed similarly to that FEM-T3 Eq. (2.21).

However, Lo (2014) showed that the rate of convergence in FEA will slow down in the presence of stress singularity and discontinuity within the domain. The poor approximate solutions of FEM using uniform mesh have revealed the poor accuracy of the simple refinement strategy, especially for the singularity problems. In the next sections, an automatic AMR scheme within the ES-FEM framework adopting constant strain element is applied to provide the elastic responses of engineering mechanics problems associated with physically instabilizing stress singularity. The three-node singular ES-FEM framework adopted the same proposed mesh adaptation is also performed for mechanics problems with arbitrary order of elastic stress singularity.

CHAPTER 3 ES-FEM-T3 AND SINGULAR ES-FEM-T3 IN ELASTIC SOLID MECHANICS

3.1 Introduction

The S-FEM models introduce "softening" effects into the conventional FEM models using the shape function values and not its gradients. Instead of taking information of nodes at the vertices inside each triangle element, S-FEM spreads out to use nodes from surrounding elements to construct smoothed strain field for the purpose of the stability, convergence and high accuracy. It is straighforward and easy-to-modify from the standard FEM without much extra computing expenses. S-FEM model is eminently suitable for a mesh of polygonal elements with arbitrarily n sides particularly the three-node triangle elements denoted to ES-FEM-T3.

Among the above S-FEM models, ES-FEM is outstanding with stable both spatially and temporally and produces super-accurate solutions compared to the original FEM in (G. Liu, Nguyen-Thoi, & Lam, 2009) and some other superior properties. Three principle features (G. Liu, 2008) as follows:

(a) Close-to-exact stiffness formulation;

(b) Coarse mesh accuracy;

(c) Simple implementation using the similar basis to a standard three-node triangular element.

However, ES-FEM is not good enough to solve the problems with domain containing discontinuities. Adopting new singular elements for the current model will be efficient in analyzing structures subjected to the difficulties associated with elastic stress singularity and discontinuity. In this method, a layer of singular five-noded elements introduced by (G. Liu, Nourbakhshnia, & Zhang, 2011) is used around the singular point and is designed to be compatible with triangular simplex (T3) elements in the remaining area. Only a node is added on the edges that directly connected to the crack tip while linear triangulars remain unchanged. This will create an combined mesh of three- and five-noded triangle elements, so-called the singular edge-based finite element method or singular ES-FEM, in which a proper order of stress singularity can

be obtained around the singular point or crack tip (L Chen et al., 2010; G. Liu, Nourbakhshnia, Chen, & Zhang, 2010). The stiffness matrix derived from a global system of discretized equations is assembled using the displacement values and not its gradients on the boundaries of SDs associated with the edges. Therefore, the integrate singular terms $r^{\lambda-1}(\lambda < 1)$ can be eliminated.

3.2 ES-FEM-T3.

3.2.1 Creation of Smoothing Domains.

The same 2D triangle element mesh with N_e elements, N_n nodes, and N_{eg} edges is generated. Then, a set N_s of "non-overlap" and "no-gap" SDs Ω_k^s will fill in the whole problem domain $\Omega = \cup_{k=1}^{N_s} \Omega_k^s$ and $\Omega_i^s \cap \Omega_j^s = \varnothing, i \neq j$.

In each SD, there are a number of "non-overlap" and "no-gap" sub-smoothing domains where $\Omega_k^s = \cup_{k=1}^{n_s} \Omega_{k,q}^s$ and $\Omega_{k,i}^s \cap \Omega_{k,j}^s = \varnothing, i \neq j$.

$\Omega_{k,q}^s$ denote to the q-th sub-smoothing domain or sub-SD, n_q is the number of sub-SDs or the number of elements supporting the smoothing domains
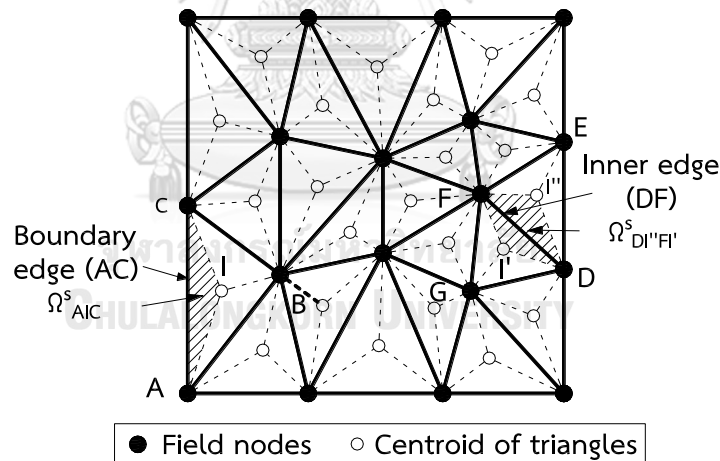
Figures 3.1 Triangle element mesh and the smoothing domains (shaded areas) encompass the edges in ES-FEM-T3 model.

The SD associated with edges is created by linking two endpoints of every edges to centre points of the surrounding elements as depicted in Fig. 3.1.

where n_q = 2, for the number of elements sharing interior edge k, n_q = 1, for the number of elements sharing boundary edge m.

3.2.2 Construction of Shape Function.

Whenever three-node triangle mesh is used, the same shape functions from the standard FEM are also applied in S-FEM as constructed in Section 2.2.2.1 a). The set of nodes contributing in the displacement interpolation formulation, however, no longer three as in standard FEM, is varying depending on how many nodes of adjacent elements supporting the smoothing domain, N^s_n.

$$\bar{u} = \sum_{i=1}^{N^s_n} N_i(x,y)\bar{d}_i = \left\{N_1 \quad N_2 \quad ... \quad N_{N^s_n}\right\}\left\{\bar{d}_1 \quad \bar{d}_2 \quad ... \quad \bar{d}_{N^s_n}\right\}^T = [N]\{\bar{d}\} \quad (3.1)$$

Note: in the general case of using any types of element, a Point Interpolation Method (G.-R. Liu & Gu, 2001), is used to construct the shape functions for n-sided polygonal elements.

3.2.3 Construction of Smoothed Strain Field

Eqs. (2.18) and (2.19) for constructing smoothed strain field through either modifying the compatible strain field from the standard FEM or using shape function values over every local SDs based on edges of triangle mesh.

A smoothing strain operator is performed over the edge-based SDs Ω^s_k resulting in constant smoothed strain fields in each SDs

$$\bar{\varepsilon}_k = \int_{\Omega^s_k} \tilde{\varepsilon}(x)\widehat{W}(x)d\Omega \quad (3.2a)$$

$$\bar{\varepsilon}_k = \int_{\Omega^s_k} L_d\bar{u}(x)\widehat{W}(x)d\Omega \quad (3.2b)$$

Note that: Eq. (3.2a) is used when $\tilde{\varepsilon}(x)$ is available.

where $\tilde{\varepsilon}(x)$ is the compatible strain field in Eq. (2.18)

$$L_d = \begin{bmatrix} \delta/\delta x & 0 \\ 0 & \delta/\delta y \\ \delta/\delta y & \delta/\delta x \end{bmatrix}, \text{ denote the matrix of derivative operations,}$$

$\widehat{W}(x)$ is a distribution/weight function needs to satisfy the following properties:

1) Positive only in the area inside the local smoothing domain Ω^s_k and zero for the other locations.

2) The unity property of $\int_{\Omega^s_k} \widehat{W}(x)d\Omega = 1$ (3.3)

The simple form of the Heaviside-type smoothing function is adopted as

$$\widehat{W}(\mathbf{x}) = \begin{cases} 1/A_k^s, & \mathbf{x} \in \Omega_k^s \cup \Gamma_k^s \\ 0 & \mathbf{x} \notin \Omega_k^s \cup \Gamma_k^s \end{cases} \tag{3.4}$$

where $A_k^s = \int_{\Omega_k^s} d\Omega = \frac{1}{3}\sum_{j=1}^{N_e^k} A_j$ is the area of SD Ω_k^s, with N_e^k denote the number of

elements contributing the edge k (N_e^k = 1 in edges on the boundary and N_e^k =2 in

edges inside), and $\frac{1}{3}A_j$ equals the area of sub-SD belong to the j-th element around

the edge k such as $A_{DI''F} = \frac{1}{3}A_{DEF}$ in Fig. 3.2.

Note: the weight function $\widehat{W}(\mathbf{x})$ vanishes only out of the domain $\left[\Omega_k^s\right] = \Omega_k^s \cup \Gamma_k^s$ to

ensure it is differentiable over Ω_k^s and applicable for Green's theorem in the next

sections.

3.2.3.1 Adopting The Compatible Strain Field

In the case that the compatible strain field is available, from Eq. (2.28)

$$\bar{\varepsilon}_k = \frac{1}{A_k^s} \int_{\Omega_k^s} \tilde{\varepsilon}(x)d\Omega \tag{3.5}$$

The smoothed strain field is piecewise constant inside every smoothing domains, it

means that:

$$\bar{\varepsilon}_k = \bar{\varepsilon}_k(x) = \bar{\varepsilon}(x_k) = \frac{1}{A_k^s} \int_{\Omega_k^s} \tilde{\varepsilon}(x)d\Omega \ , \ \forall x \in \Omega_k^s \tag{3.6}$$

Note: Eq. (3.6) shows formulation of taking area averaged compatible strains over SDs

Ω_k^s and only applicable for constant strain element mesh.

3.2.3.2 Adopting The Flux of The Displacement Field

In general, smoothed strain field can be constructed by using the flux of the

displacement field as follows.

With the assumption of continuous displacement field along the boundary Γ_k^s in ES-

FEM-T3 model and the differentiation of weight function $\widehat{W}(\mathbf{x})$ as mentioned above,

we can apply Green's divergence theorem into the second term in Eq. (3.2):

$$\bar{\varepsilon}_k = \int_{\Omega_k^s} L_d\left[\bar{u}(x)\right]\widehat{W}(\mathbf{x})d\Omega = \frac{1}{A_k^s}\int_{\Gamma_k^s} L_n(x)\bar{u}(x)d\Gamma - \int_{\Omega_k^s} L_d\left[\widehat{W}(\mathbf{x})\right]\bar{u}(x)d\Omega$$
$$= \frac{1}{A_k^s}\int_{\Gamma_k^s} L_n(x)\bar{u}(x)d\Gamma \tag{3.7}$$

Note: the second term at the second line in Eq. (3.7) vanishes because $\widehat{W}(\mathbf{x})$ is constant in smoothing domain Ω_k^s.

where $L_d = \begin{bmatrix} \delta/\delta x & 0 \\ 0 & \delta/\delta y \\ \delta/\delta y & \delta/\delta x \end{bmatrix}$ denote the matrix of derivative operations $\qquad$ (3.8)

$L_n(\mathbf{x}) = \begin{bmatrix} n_x & 0 \\ 0 & n_y \\ n_y & n_x \end{bmatrix}$ contains components of the outward normal vector on boundary

Γ_k^s as depicted in Fig. 3.2.
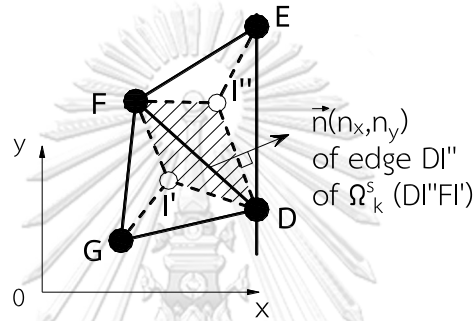
Figure 3.2 The x-, y- outward normal vector (n_x, n_y), for the edge DI'' in the smoothing domain (DI''FI')

Eq. (3.7) is a line integration along the boundary Γ_k^s of the SD Ω_k^s. In other words, it is the computation of the flux displacement field accross the boundary of SD Ω_k^s. Similarly, it is intended to be piecewise constant in smoothing domains:

$$\bar{\varepsilon}_k = \bar{\varepsilon}_k(\mathbf{x}) = \bar{\varepsilon}(\mathbf{x}_k) = \frac{1}{A_k^s} \int_{\Gamma_k^s} L_n(\mathbf{x})\bar{u}(\mathbf{x})d\Gamma, \quad \forall \mathbf{x} \in \Omega_k^s \qquad (3.9)$$

Note: Eq. (3.9) for a general types of elements being used in various S-FEM models in comparison with Eq. (3.7) that only applicable to three-node element.

3.2.4 Smoothed Strain–Displacement Matrix

Substituting Eq. (3.1) into Eq. (3.9), the smoothed strain then becomes:

$$\bar{\varepsilon} = \sum_{i=1}^{N_n^s} \bar{B}_i(x,y)\bar{d}_i = \begin{bmatrix} \bar{B}_1 & \bar{B}_2 & \dots & \bar{B}_{N_n^s} \end{bmatrix} \begin{Bmatrix} \bar{d}_1 & \bar{d}_2 & \dots & \bar{d}_{N_n^s} \end{Bmatrix}^T = \begin{bmatrix} \bar{B} \end{bmatrix} \{\bar{d}\} \quad (3.10)$$

Where $\bar{B}_i(x,y)$ is the "smoothed strain-displacement" matrix of node i-th contributing into overall smoothed strain–displacement matrix $\begin{bmatrix} \bar{B} \end{bmatrix}$ of SD Ω_k^s.

As mentioned before, N^s_n contains the set containing field nodes which supporting the SD Ω^s_k (e.g. ES-FEM model using three-node triangle elements in Fig. 3.1, $N_{n,s}$ = 3 for the boundary edge m which is (A, B and C) from triangular ΔABC only, and $N_{n,s}$ = 3 for the interior edge k which is (D, E, F and G) from the triangle ΔDEF and ΔFGD. The smoothed strain–displacement matrix $\bar{B}_i$ becomes

$$\bar{B}_i(x_k) = \frac{1}{A^s_k} \int_{\Gamma^s_k} L_n(x)N_i(x)d\Gamma = \begin{bmatrix} \bar{b}_{ix}(x_k) & 0 \\ 0 & \bar{b}_{iy}(x_k) \\ \bar{b}_{iy}(x_k) & \bar{b}_{ix}(x_k) \end{bmatrix} \tag{3.11}$$

with

$$\bar{b}_{ix(y)}(x_k) = \frac{1}{A^s_k} \int_{\Gamma^s_k} n^k_{x(y)}(x)N_i(x)d\Gamma \tag{3.12}$$

Eq. (3.11) can be performed by applying a Gauss integration technique. In essense, a Gauss-point is good enough for computing the line integration along each boundaries Γ^s_k, then the formulation reduces to a summation form of

$$\bar{b}_{ix(y)}(x_k) = \frac{1}{A^s_k} \sum_{p=1}^{n^s_\Gamma} n^k_{x(y),p}(x)N_i\left(x^{Gauss}_p\right)l_p \tag{3.13}$$

where n^s_Γ denote the total number of boundary segments $\Gamma^s_k = \sum \Gamma^s_{k,p}$, x^{Gauss}_p is the coordinates of the mid-point (Gauss-point) of p-th the boundary segment $\Gamma^s_{k,p}$, $n_{x(y),p}$ and l_p denote for the unit normal and the length of the p-th boundary segment $\Gamma^s_{k,p}$ Up to this point, it is straightforward to obtain the formulation of $\bar{B}_i$ using the origin compatible strain-displacement matrix $\tilde{B}_i(x)$ from the standard FEM:

$$\bar{B}_i = \frac{1}{A^s_k} \int_{\Gamma^s_k} L_n(x)N_i(x)d\Gamma = \frac{1}{A^s_k} \int_{\Omega^s_k} L_p(x)N_i(x)d\Omega = \frac{1}{A^s_k} \int_{\Omega^s_k} \tilde{B}_i(x)d\Omega \tag{3.14}$$

Eq. (3.14) shows that the $\bar{B}_i$ matrix is the averaged formulation of the compatible matrix $\tilde{B}_i(x)$ matrix over the smoothing domain Ω^s_k.

$\tilde{B}_i(x)$ will be piecewise constant such that Eq. (3.14) for constructing the smoothed $\bar{B}_i$ matrix can be transformed into a so-called area-weighted average formulation as follows:

$$\bar{B}_i = \frac{1}{A^s_k} \sum_{j=1}^{N^k_e} \frac{1}{3} \tilde{B}_j A_j \tag{3.15}$$

where the $\tilde{B}_j$ matrix denote compatible strain-displacement matrix of the j-th element surrounding edge k and obtained by using Eq. (2.19).

$A_k^s = \int_{\Omega_k^s} d\Omega = \frac{1}{3} \sum_{j=1}^{N_e^k} A_j$ denote the area of SD Ω_k^s and $\frac{1}{3} A_j$ denote the area of sub-

SD belong to the j-th element surrounding the edge k such as $A_{DI''F} = \frac{1}{3} A_{DEF}$ in Fig. 3.2

Note:

(1) The Eq. (3.15) is simple and easy-to-implement based on available FEM-T3 model. It is applicable, however, for constant triangle elements with linear interpolation shape functions. The S-FEM models that adopting arbitrary n-sided elements or higher-order interpolation shape functions, the general Eq. (3.11) should be performed for computing the smoothed $\bar{B}_i$ matrix.

(2) In triangle mesh, the size of matrix $\tilde{B}_j$ is (3×6 row$\times$column) in the standard FEM model. In ES-FEM, however, the size of the smoothed matrix $\bar{B}_i$ can vary in a model and depends on the type of smoothing domain (SD). For example, $\bar{B}_i$ for interior SD is a (3×8) matrix and for boundary SD is a (3×6) matrix in a ES-FEM model, such as, depicted by the Fig. 3.2 the (3×8) matrix $\tilde{B}_{DF}$ for the interior SD based on interior edge DF will bring information of four-node D, E, F, G, and similar for the (3×6) matrix $\tilde{B}_{AC}$ for the boundary SD based on boundary edge AC will bring information of only three-node A, B, C.

3.2.5 Smoothed Galerkin Weak Form

The ES-FEM that using the Galerkin weak form in terms of smoothed strain field instead of compatible strain field or smoothed Galerkin weak form (G.-R. Liu, 2009) reads

$$\sum_{k=1}^{N_s} A_k^s \left(\frac{1}{A_k^s} \int_{\Gamma_k^s} L_n(x)\delta\bar{u}(x)d\Gamma \right)^T D \left(\frac{1}{A_k^s} \int_{\Gamma_k^s} L_n(x)\bar{u}(x)d\Gamma \right) - \int_\Omega \delta\bar{u}^T b d\Omega - \int_\Gamma \delta\bar{u}^T t d\Gamma = 0$$

or $$\sum_{k=1}^{N_s} A_k^s \delta\bar{\varepsilon}_k^T D\bar{\varepsilon}_k - \int_\Omega \delta\bar{u}^T b d\Omega - \int_\Gamma \delta\bar{u}^T t d\Gamma = 0 \qquad (3.16)$$

where N_s denotes the number of SD, or number of edges N_{eg}, in the whole problem domain of ES-FEM, A_k^s denotes the area of the k-th SD, b is the body load acting over the whole domain and t is the external traction load defined on the Neumann boundary.

3.2.6 Discretized Linear System of Equations.

Firstly, we obtain a similar discretized system of equations for the ES-FEM with those of FEM-T3. The only difference is replacing the standard matrix $\tilde{K}$ by the smoothed matrix as follows:

$$\bar{K}\bar{d} = \tilde{f} \tag{3.17}$$

In which the $\bar{K}$ matrix equals

$$\bar{K} = \sum_{k=1}^{N_s} \bar{K}^k \tag{3.18}$$

and its entries is computed by:

$$\bar{K}_{IJ} = \sum_{k=1}^{N_s} \int_{\Omega_k^s} \bar{B}_I^T D \bar{B}_J \, d\Omega = \sum_{k=1}^{N_s} \bar{B}_I^T D \bar{B}_J A_k^s t \tag{3.19}$$

where $N_s = N_{eg}$ is the number of SDs or edges over the whole domain of ES-FEM-T3, $\bar{K}^k$ denotes the elemental stiffness matrix associated with SD Ω_k^s, $\bar{K}_{IJ}$ is the entries of $\bar{K}$ that relating the nodes I to J. The global stiffness matrix $\bar{K}$ of ES-FEM-T3, however, is assembled over SDs instead of individual triangle elements

This global smoothed stiffness matrix $\bar{K}$ is also extremely sparse but may not as much as in the $\tilde{K}$ matrix in the standard FEM. The reason is that it consider more nodes in contributing to the elemental, namely SD, stiffness matrices compared with the original FEM-T3 counterparts.

The nodal load vector keeps unchange Eq. (2.21) as in the standard FEM.

3.3 Singular ES-FEM-T3.

In linear fracture analysis, infinite stress value will occur at the crack tip. Of the numerical method, the standard FEM uses a (quadratic) 6-node crack-tip element to approximate the stress singularity where the mid-points are shifted by a distance one-fourth edge length toward the crack tip. An isoparametric mapping procedure is then applied to create the singular field by (Olgierd Cecil Zienkiewicz, Taylor, Taylor, & Taylor, 2000). However, no mapping is required for the singular ES-FEM using combined mesh of three- and five-node elements. A simple point interpolation method adding basis functions with proper order of power terms make possible creating the singular stress field around the crack tip in the singular ES-FEM method.

3.3.1 Singular Stress Field at The Crack-Tip

A crack body as depicted in Fig. 3.3 is discretized using a layer of five-noded triangle elements surrounding the crack-tip and the normal three-node triangle elements in the remaining area. Additional nodes are presented on every edges that directly connect to the crack tip.

● Field nodes   ○ Centroid of triangles
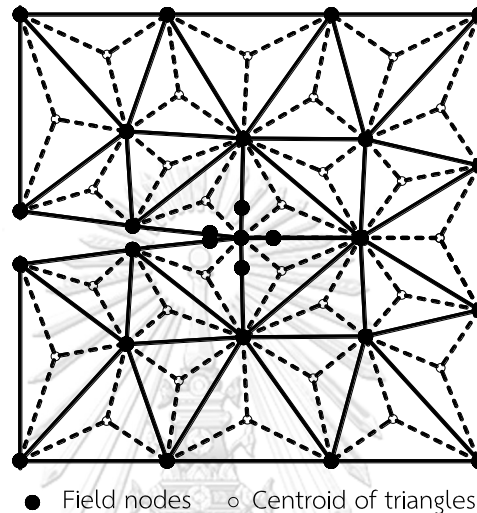
Figures 3.3 Triangular mesh with layer of five-node elements in singular ES-FEM-T3.

The construction of singular stress field performed by: Firstly, interpolating the displacement value along the crack-tip edge by adopting the enriched linear PIM and then, the displacement field inside the singular elements will be constructed.

3.3.1.1 Displacement Interpolation along The Crack-Tip Edge

It is also noted that the additional nodes can be any location on the crack tip edge in the singular ES-FEM model compared with an fixed position of one-fourth edge length in the conventional FEM illustrated in Fig. 3.4.
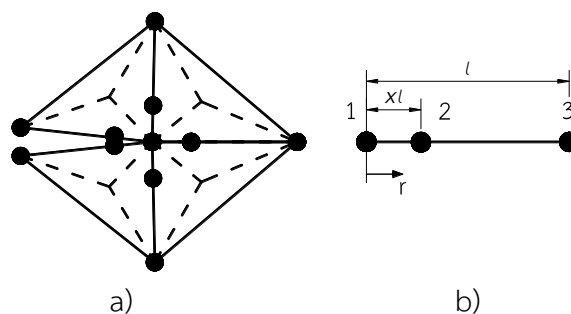

a)   b)

Figure 3.4 Additional point on the crack tip edge

The displacement field, u, along the crack-tip edge is approximated by:

$$u(x) = P^T(x)a = a_0 + a_1 r + a_2 r^\lambda \tag{3.20}$$

where the radial coordinate r with origin point at the crack-tip and $0 \le r \le l$ in Fig. 3.4 b, and a_i (i = 0, 1, 2) are the unknown coefficients, $1/2 \le \lambda < 1$ is a singularity parameter computed from the characteristic equations depending on the vertex angular and the BCs on two angle faces as in Section 2.1.3.

After replacing the nodal coordinates into Eq. (3.20), then

$$u_1 = a_0 ; (r = 0 \text{ at node 1})$$

$$u_2 = a_0 + a_1 \chi l + a_2(\chi l)^\lambda ; (r = \chi l \text{ at node 2}) \tag{3.21}$$

$$u_3 = a_0 + a_1 l + a_2 l^\lambda ; (r = l \text{ at node 3})$$

or in the matrix form: $\quad\quad\quad d = Ca, \tag{3.22}$

with $d = \{u_1 \quad u_2 \quad u_3\}^T$ contains nodal displacements and matrix (3x3) C of the radial coordinates at nodes

$$C = \begin{bmatrix} 1 & 0 & 0 \\ 1 & \chi l & (\chi l)^\lambda \\ 1 & l & l^\lambda \end{bmatrix} \tag{3.23}$$

where l denote the edge length and the ratio of the edge 1-2 over the edge 1-3 denoted by χ (with $0 \le \chi \le 1$)

Solving the Eq. (3.22) for vector and substituting them back into Eq. (3.21), then

$$u(x) = P^T(x)C^{-1}d = \Phi(x)d \tag{3.24}$$

where $\Phi = [\Phi_1 \quad \Phi_2 \quad \Phi_3]$ stores shape functions for nodes on the crack tip edge is defined as follows:

$$\Phi_1 = 1 + \frac{r^\lambda(\chi - 1) + l^{\lambda-1}(1 - \chi^\lambda)r}{(\chi l)^\lambda - \chi l^\lambda} ; \Phi_2 = \frac{r^\lambda - l^{\lambda-1}r}{(\chi l)^\lambda - \chi l^\lambda} ; \Phi_3 = \frac{l^{\lambda-1}\chi^\lambda r - \chi r^\lambda}{(\chi l)^\lambda - \chi l^\lambda} \tag{3.25}$$

As already studied, χ can take any value in the range (0-1) opposite to that in FEM approach using the quarter point elements which is fixed to equal 1/4. To be simple and, χ is set to be 1/4, then the shape functions change to

$$\Phi_1 = 1 - \left(\frac{r}{l}\right)^\lambda \cdot \frac{4^{\lambda-1}}{1-4^{\lambda-1}} + \left(\frac{r}{l}\right) \cdot \frac{\left(4^\lambda - 1\right)}{1-4^{\lambda-1}}$$

$$\Phi_2 = \left(\frac{r}{l}\right)^\lambda \cdot \frac{4^\lambda}{1-4^{\lambda-1}} - \left(\frac{r}{l}\right) \cdot \frac{4^\lambda}{1-4^{\lambda-1}} \tag{3.26}$$

$$\Phi_3 = -\left(\frac{r}{l}\right)^\lambda \cdot \frac{4^{\lambda-1}}{1-4^{\lambda-1}} - \left(\frac{r}{l}\right) \cdot \frac{1}{1-4^{\lambda-1}}$$

For fracture mechanics problems with in-line crack faces, $\lambda = 1/2$ and the shape functions become

$$\Phi_1 = 1 + 2\frac{r}{l} - 3\sqrt{\frac{r}{l}}; \; \Phi_2 = -4\frac{r}{l} + 4\sqrt{\frac{r}{l}}; \; \Phi_3 = 2\frac{r}{l} - \sqrt{\frac{r}{l}} \tag{3.27}$$

The Φ_i owns basic properties of a normal shape function, namely linear reproducibility, partition of unity and Kronecker delta properties. The shape functions with linear dependence are enriched with a term of $\sqrt{r}$ in r-direction that actually produces stress (or strain) singularity field with an exponent of 1/2.

Integration for the term of $r^{\lambda-1}$ can be removed since no derivative of shape functions will be performed in S-FEMs. In addition, no mapping procedure is required compared to the standard FEM counterparts.

3.3.1.2 Creation of Displacement Field Within A Five-Node Triangle Element.

As already presented, in the singular ES-FEM-T3, only the edges that directly connect to the singular point are added one node with one-fourth distance from the original (singular) point. The same nodal shape functions derived in Eq. (3.26) can be properly performed in this singular element. The displacement interpolation uses the enriched form as formulated in Eq. (3.21) in the radial direction, while it is interpolated with linear dependence in the tangential direction that will assure the compatibility along the two-node edge of crack-tip elements.

Now, we consider the singular element 1-4-2-3-5 as depicted in Fig. 3.5. The node 6 and 7 denote to the mid-points of lines 4-5 and 2-3, respectively. Then the displacements can be obtained by averaging those from the field nodes (because of the assumption of linear dependence on the tangential direction) by

$$u_6 = \frac{1}{2}\left(u_4 + u_5\right); \; u_7 = \frac{1}{2}\left(u_2 + u_3\right) \tag{3.28}$$

Note that: the linear point interpolation method is taken into account in this case then linear interpolation inside the singular element can take the Eq. (3.28) at any point.
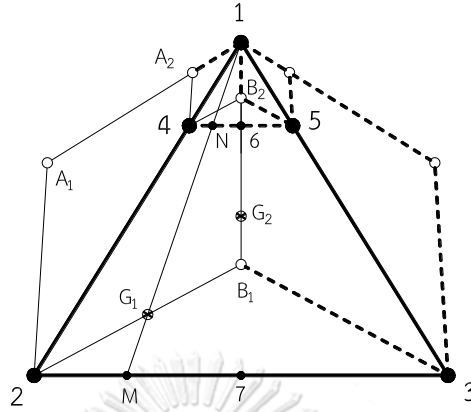
Figures 3.5 Two layers of singular smoothing domains in singular ES-FEM-T3.

Along the arbitrary radial line 1-N-M, displacement is obtained using the Eq. (3.24) as

$$u = \Phi_1 u_1 + \Phi_2 u_N + \Phi_3 u_M \tag{3.29}$$

with

$$u_N = \left(1 - \frac{l_{N-4}}{l_{5-4}}\right) u_4 + \frac{l_{N-4}}{l_{5-4}} u_5, \; u_M = \left(1 - \frac{l_{M-2}}{l_{3-2}}\right) u_2 + \frac{l_{M-2}}{l_{3-2}} u_3 \tag{3.30}$$

where l_{i-j} denotes for the distance from point i to j. Similar triangle rule leads to $\frac{l_{N-4}}{l_{5-4}} = \frac{l_{M-2}}{l_{3-2}} = \alpha$, after substitute Eq. (3.30) into Eq. (3.29), we finally get the general form

$$u = \Phi_1 u_1 + (1-\alpha)\Phi_3 u_2 + \alpha\Phi_3 u_3 + (1-\alpha)\Phi_2 u_4 + \alpha\Phi_2 u_5 \tag{3.31}$$

In matrix form: $\qquad\qquad u = Nd \tag{3.32}$

where N contains shape functions for degree of freedoms or DOFs of singular element and $N = \left\{ N_1 = \Phi_1; \; N_2 = (1-\alpha)\Phi_3; \; N_3 = \alpha\Phi_3; \; N_4 = (1-\alpha)\Phi_2; \; N_5 = \alpha\Phi_2 \right\}$ with Φ_i (i = 0, 1, 2) are the same as above sections.

In the special cases of interpolating along the element edge such as line 1-4-2, 1-5-3 or line 1-B2-B1, the value of α equal to 0, 1, 1/2, respectively. After substituting into Eq. (3.31), we obtain the corresponding shape functions. Therefore, Eq. (3.31) is the general form for interpolating the displacement field within the present singular element.

3.3.2 Smoothing Domains in The Singular ES-FEM-T3

In the present ES-FEM-T3, strain smoothing domains or SDs are created encompassing edges in triangle mesh. Each triangle element contains three sub-smoothing domains or sub-SDs corresponding to their three edges and every two sub-SDs from adjacent elements form a edge-based SD. In these singular elements, similar SDs can be constructed. Multi-layer SDs, however, are needed to better approximate the presence of the singularity stress. As already studied, two layers of singular smoothing domains (singular SDs) are good enough to assure both stability and accuracy in approximating the singular term around the crack-tip. In each five-node element, a smaller layer of SDs established by connecting two additional nodes and the center point of the smaller triangle close to the singular point Fig. 3.5, namely triangle $1-4-B_2-1$ and $1-B_2-5-1$. The second layer that is quadrilateral-shaped and next to (outside) the first layer, namely quadrangle $4-B_2-B_1-2-4$ and $B_2-5-3-B_1-B_2$. The last one is the normal s-SD, namely $2-B_1-3-2$, which ensures the conformity of normal SD associated with the remaining edge.

In the three-node triangle ES-FEM model, the shape function is linearly dependent along the boundaries of normal SDs. Therefore, one Gauss-point is good enough for approximately integrating on every boundary segments. However, more than one Gauss-point are required on the boundary segments of the singular SDs in the singular model because of the complex variation of the term r^λ in the displacement field along these boundary segments.

For example, we now consider the edge of $2B_1$ to be intergral. It has the Gauss-point G_1 on the boundary in the tangential direction, and also located on the line 1-N-M as depicted in Fig. 3.5, the displacement is interpolated using the general Eq. (3.31). For the Gauss-point G_2 on the boundary B_1B_2 in the radial direction, the general Eq. (3.31) with $\alpha = 1/2$ will be considered.

3.3.3 The Smoothed Stiffness Matrix of The Singular Method

The smoothed stiffness matrix of the singular model can be constructed using two types of SDs: (1) normal SDs which are not directly related to the crack-tip point (computed in a similar fashion as section 3.2.4) and (2) singular smoothing domains or singular SDs directly related to the crack-tip point. For SDs connected to the crack tip, there are two layers of singular SDs per edge that will effectively capture the singular property.

The smoothed strain–displacement matrix of each layer of singular SDs $\Omega_k^{s,a}$ (a =1, 2), is computed as

$$\bar{B}_i^a = \begin{bmatrix} \bar{b}_{ix}^a & 0 \\ 0 & \bar{b}_{iy}^a \\ \bar{b}_{iy}^a & \bar{b}_{ix}^a \end{bmatrix} \tag{3.33}$$

with
$$\bar{b}_{ix(y)}^a(x_k) = \frac{1}{A_k^{s,a}} \int_{\Gamma_k^{s,a}} N_i(x) n_{x(y)}^{k,a}(x) d\Gamma \tag{3.34}$$

where $A_k^{s,a}, \Gamma_k^{s,a}$ denote the area and the boundary of the a-th layer of the singular SD $\Omega_k^{s,a}$, respectively, the shape functions $N_i(x)$ in Eq. (3.25) are adopted in this case, $n_{x(y)}^{k,a}$ denotes the unit normal vector of the boundary segment $\Gamma_k^{s,a}$

Similarly, we apply the Gauss integration along the segments of boundary $\Gamma_k^{s,a}$, then

$$\bar{b}_{ix(y)}^a = \frac{1}{A_k^{s,a}} \sum_{p=1}^{n_\Gamma^s} \left[\sum_{b=1}^{n_{Gauss}} w_{p,b} n_{p,x(y)}^{k,a}(x) N_i\left(x_{p,b}^{Gauss}\right) \right] \tag{3.35}$$

where n_{gauss} denote the number of Gauss points for each boundary segment, $w_{p,b}$ is the corresponding weight coefficient of that Gauss points, $x^{gauss}_{p,b}$ denote the b-th Gauss-point of the p-th boundary segment of $\Gamma_k^{s,a}$ and n_Γ^s is the number of boundary segments of $\sum_{p=1}^{n_\Gamma^s} \Gamma_{k,p}^{s,a} = \Gamma_k^{s,a}$.

Note: the number of Gauss-points required for the numerical integration in Eq. (3.35) now is not only one as that in the standard ES-FEM-T3. Parameter study has been performed together with the application of the singular ES-FEM-T3 to obtain an approximate number of Gauss-points that is good enough for such integration (L Chen, Liu, Jiang, Zeng, & Zhang, 2011). Three Gauss-points on every boundary segment of the

singular SDs are sufficient to provide a good approximation, n_{gauss} = 3 is used in this study.

A similar procedure for obtaining the discretized linear system of equations as well as the nodal load vector from the ES-FEM-T3 is implemented in the present singular model.
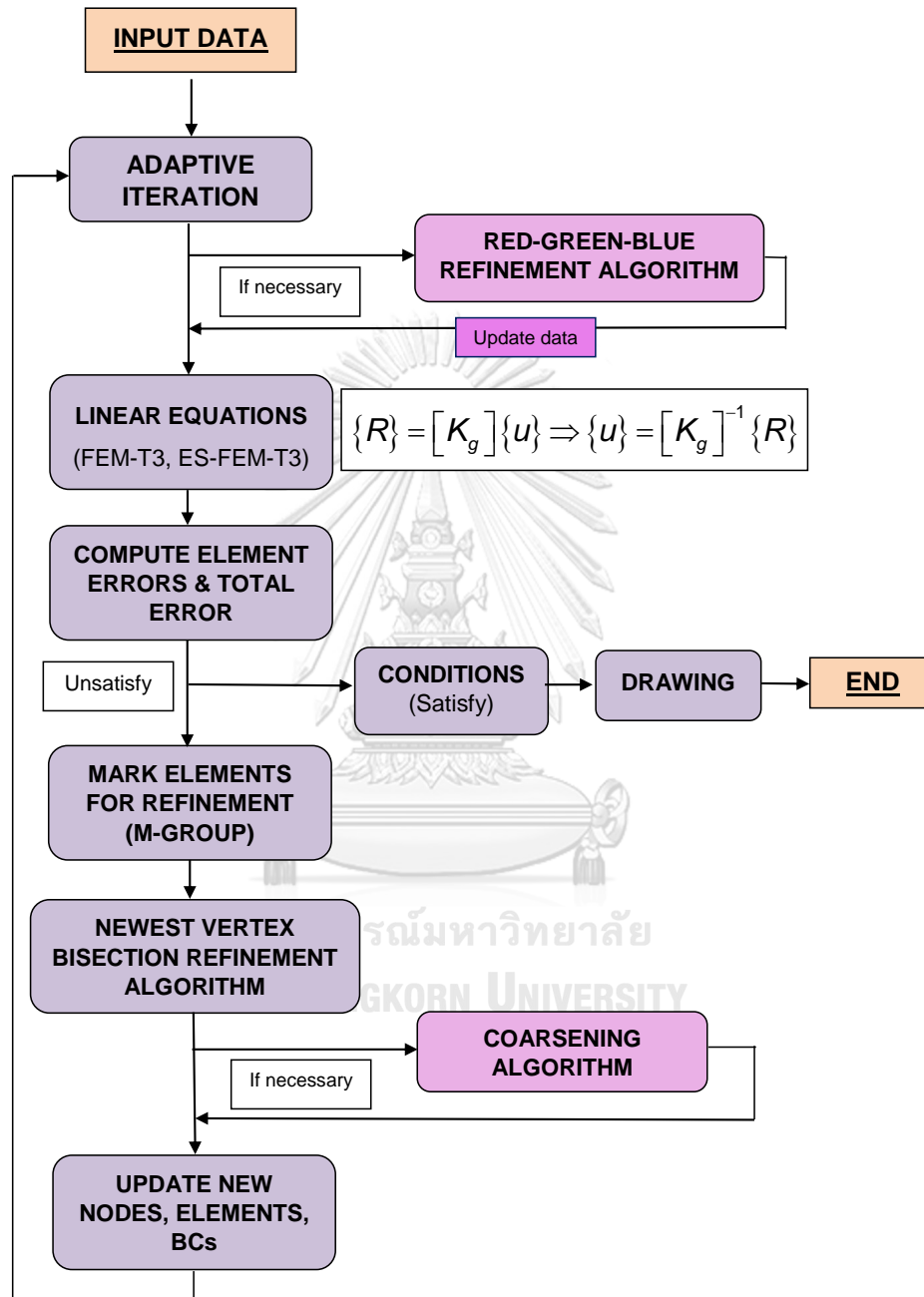
CHAPTER 4 AUTOMATIC ADAPTIVE FEM-T3 AND ES-FEM-T3

4.1 Introduction

Under the adaptive analysis, better solutions can be achieved in a controlled computational effort. In this study, local refinement of three-node triangle elements accompanied by subdivision of neighbor simplices along the longest edge or LE to ensure conformity. Such LE partitions of triangles introduced by (Rosenberg & Stenger, 1975) and (M.-C. Rivara & Iribarren, 1996) for maintaining the conformity of the mesh and eliminating degradation in mesh quality, simultaneously. This technique, however, leads to by-product effects which induce unnecessary refinement for surrounding elements from the target subdivided elements. Suárez, Plaza, and Carey (2008) concluded in their studies that the adjacent propagation inherent to LE refinement does not make a significant change in the results, especially in 2D applications. Moreover, this adaptive scheme can be effectively performed in both the standard FEM-/ES-FEM-T3 models because they use the same triangular element. A parent triangle element can be sub-divided into several children triangle elements using the so-called newest vertex bisection technique. The process can continue until a convergence of the results is obtained. As a result, the implementation of the adaptive standard FEM-/ES-FEM-T3 obviously provides an efficient mesh generation with higher-level accuracy of solutions and reduces the requirement for consuming computational resources.

4.2 Adaptive Algorithm Implementation

4.2.1 Flowchart

INPUT DATA

ADAPTIVE
ITERATION

RED-GREEN-BLUE
REFINEMENT ALGORITHM

If necessary

Update data

LINEAR EQUATIONS
(FEM-T3, ES-FEM-T3)

$$\{R\} = \left[K_g\right]\{u\} \Rightarrow \{u\} = \left[K_g\right]^{-1}\{R\}$$

COMPUTE ELEMENT
ERRORS & TOTAL
ERROR

Unsatisfy

CONDITIONS
(Satisfy)

DRAWING

END

MARK ELEMENTS
FOR REFINEMENT
(M-GROUP)

NEWEST VERTEX
BISECTION REFINEMENT
ALGORITHM

COARSENING
ALGORITHM

If necessary

UPDATE NEW
NODES, ELEMENTS,
BCs

4.2.2 Adaptive Formulation

The refinement indicators η_I, which is the value of error estimators from the aforementioned sections, will be used to seek a group of elements $\Omega_I \in \Omega$ for refinement. In our study, we use the well-known Dorfler criterion (Dörfler, 1996) to find the minimal set $\Omega_M \in \Omega$ such that:

$$\theta \sum_{\Omega_I \in \Omega} \eta_I^2 \leq \sum_{\Omega_I \in \Omega_M} \eta_I^2 \qquad (4.1)$$

where the parameter $\theta \in (0,1)$ means that if $\theta \to 1$ the mesh is almost uniformly refined (e.g. Almost all of elements are stored for refinement and if $\theta \to 0$ means that a highly adapted mesh will be performed. As mentioned before, this case will restrict the unnecessary refinement for surrounding elements. With this criterion, a new mesh Ω' is obtained by subdividing at least the marked elements assumed M-Group $\Omega_M \in \Omega$ in order to reduce total numerical errors of the whole domain.

4.2.3 Criterion for Stopping Adaptive Iteration

In mechanics problems with the presence of singular point, no amount of mesh refinement is enough to capture the correct solution. The very small sizes of elements at that point will be seen and cost a lot for analyses may very expensive. In order to prevent excessively expensive analyses of those models, we can set up a minimum element size constraint or a maximum number of elements for the given problem domain. On the other hand, the relative error indicators in some specified norms are the most important results that we need to concern. Criterion Equations are summarized as follows:

$$h_{\Omega_I \in \Omega} \leq h_{\min} \qquad (4.2)$$

$$N_e \geq N_{e,\max} \qquad (4.3)$$

$$e_\Omega \leq e_{\min} \qquad (4.4)$$

Whenever one of the above Equations reached, the adaptive analysis will stop and the previous results will be reported.

4.2.4 Newest Vertex Bisection Technique.

An original triangle may be either divided into four child triangles by linking the mid-points of their edges or bisected by connecting the mid-point of the longest edge to

the opposited vertes. The former, so-called RGB technique in the next section, possibility obviously produces similar triangles as discussed in (Verfürth, 1994), while the second one may increasingly lead to a distorted mesh. Fortunately, the longest-edge bisection so-called Newest Vertex Bisection is to divide only the longest edge of elements (M. C. Rivara, 1984) which keeps away from producing triangles with smaller angles. There are four types of partitioning a parent element into so-called child elements which are formed of lines connecting the newest vertex to the mid-point of reference edge as in Fig. 4.1
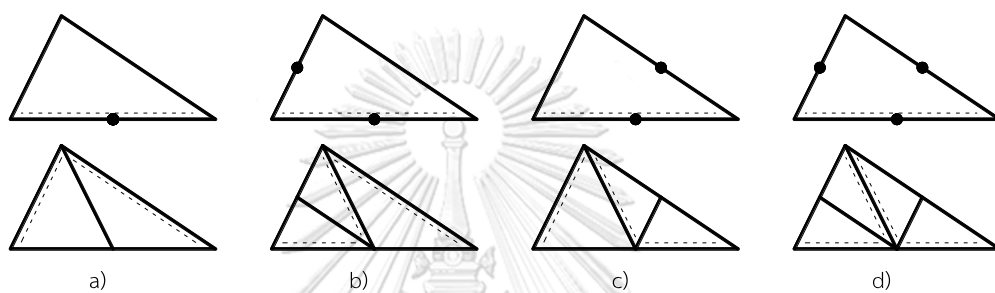

Figure 4.1 Refinement by newest vertex bisections: A triangle element with four cases of refinement, but at least the longest or reference edge is marked for refinement (in upper line). After refinement, the element is divided into 2 (a), 3 (b, c) and 4 (d) children triangles (bottom). Note that: the reference edges are added by the dash-lines

All these strategies, however, need to be modified through rules to solve the hanging nodes. The condition reads as follows, any two triangles in domain Ω share at most a common edge or a common vertex. The simplest and most efficient way that can be applied for triangular meshes is to introduce auxiliary bisected triangles shown in Fig. 4.2
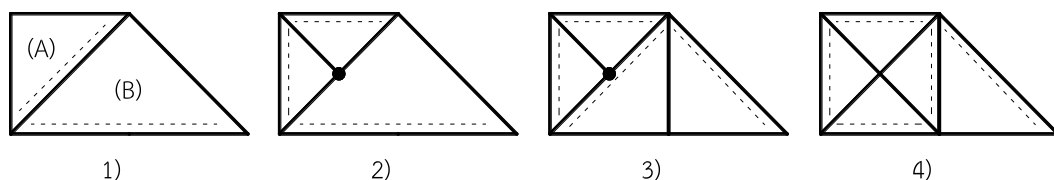

Figure 4.2 The Propagation of Newest Vertex Bisection Technique: The element (A) is marked for refinement. Bisection of the element (A) leads to a hanging node as in step (2). To avoid hanging nodes, the element (B) need to be refined and at least the

reference edge, this is as the case (b) in Fig. 4.1 and the results as in step (4). Note that: the reference edges are added by the dash-lines.

Fortunately, the adjacent propagation owing to LE refinement does not make considerable changes in the results, especially in 2D problems. Although the trends of the element excess keep extending, it is slower as refinement proceeds. It is suggested that, however, there should be appropriate modifications before applying in 3D models. Note that the more extensive refinement area the smaller number of marked elements for a single refinement step might reduce the propagation effects.
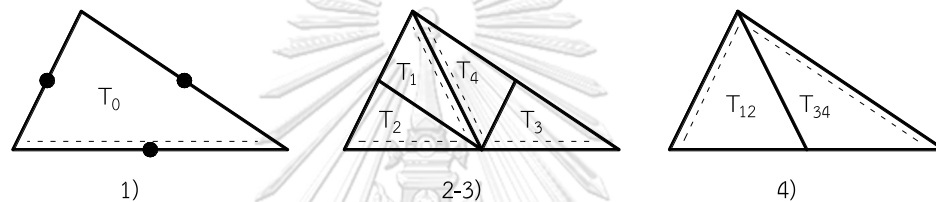
4.2.5 Coarsening Mesh Technique

Figure 4.3 Coarsening is one step back from the refinement of newest vertex bisection: Assume the triangle is marked for all three edges as in step (1) and result in 4 children elements step 2 & 3). The coarsening algorithm only unify 1 step back as step 4)

The coarsening algorithm introduced by (Long Chen & Zhang, 2010) can select a group of elements for coarsening and clear the redundant memory like former nodes. In addition, the algorithm also can update all input data in order to conform with the current mesh after coarsening such as the boundary conditions or the connectivities, etc.

4.2.6 Error Assessment in FEM-T3 and ES-FEM-T3 Models.

A mathematical discretization of continuous physical problems in FEM-T3 will introduce a discretization error into the approximate solutions. After solving above system of Equations, we obtain the numerical solution ($\tilde{u}$, $\tilde{\sigma}$) in FEM or ($\bar{u}$, $\bar{\sigma}$) in ES-FEM which differ from the exact values (u, σ) and the amount of difference is called error as

In terms of displacements: $e_d = u - \tilde{u}$ (or $u - \bar{u}$) $\hspace{3cm}$ (4.5a)

In terms of stresses: $e_\sigma = \sigma - \tilde{\sigma}$ (or $\sigma - \bar{\sigma}$) (4.5b)

The pointwise formulation of errors as shown in Eqs. (4.5a) and (4.5b) is too general to evaluate. In order to evaluate this kind of error, some mathematical error estimation techniques have been adopted. The most famous one is a simple recovery-based error estimator using the gradient recovery technique. A continuous stress field will be constructed which is demonstrated to be more accurate than the above interelement discontinuous stress field. This improved stress field can be obtained through several projection techniques (e.g. least squares smoothing or a nodal averaging of the element stresses). The exact solution is represented by this continuous solution so that the discretization error can be easily evaluated. This error estimator is called the posterior error estimator.

4.2.6.1 Global Recovery-Based Error Estimator in L2- Norm and Energy Norm.

The energy norm was proposed by (Olgierd Cecil Zienkiewicz et al., 1977) for studying a quantitative study of the error and convergence rate of numerical methods. Either errors in energy norm or L2-norm is performed associated with triangle elements. Therefore, it is applicable both for the FEM-/ES-FEM-T3 models.

The total ZZ-type error estimator

$$\eta_Z = \left(\sum_{l=1}^{N_e} \eta_l^2 \right)^{1/2}$$ (4.6)

where η_l is recovery-based error indicator of the l-th triangle element in the domain for the FEM-/ ES-FEM-T3 models and is computed by:

For the energy norm:

$$\eta_l = \left\| \tilde{\sigma} - \tilde{\sigma}^R \right\|_{E(\Omega_l)} = \left[\int_{\Omega_l} \left(\tilde{\sigma} - \tilde{\sigma}^R \right)^T D^{-1} \left(\tilde{\sigma} - \tilde{\sigma}^R \right) d\Omega \right]^{1/2}$$ (FEM-T3) (4.7a)

$$\eta_l = \left\| \bar{\sigma} - \bar{\sigma}^R \right\|_{E(\Omega_l)} = \left[\int_{\Omega_l} \left(\bar{\sigma} - \bar{\sigma}^R \right)^T D^{-1} \left(\bar{\sigma} - \bar{\sigma}^R \right) d\Omega \right]^{1/2}$$ (ES-FEM-T3) (4.7b)

For L2- norm:

$$\eta_l = \left\| \tilde{\sigma} - \tilde{\sigma}^R \right\|_{L^2(\Omega_l)} = \left[\int_{\Omega_l} \left(\tilde{\sigma} - \tilde{\sigma}^R \right)^T \left(\tilde{\sigma} - \tilde{\sigma}^R \right) d\Omega \right]^{1/2}$$ (FEM-T3) (4.8a)

$$\eta_I = \left\| \bar{\sigma} - \bar{\sigma}^R \right\|_{L^2(\Omega_I)} = \left[\int_{\Omega_I} \left(\bar{\sigma} - \bar{\sigma}^R \right)^T \left(\bar{\sigma} - \bar{\sigma}^R \right) d\Omega \right]^{1/2} \quad \text{(ES-FEM-T3)} \qquad (4.8b)$$

where $\tilde{\sigma}$ and $\bar{\sigma}$ are the numerical solution for stresses obtained using the FEM-/ES-FEM-T3, respectively, $\tilde{\sigma}^R$ and $\bar{\sigma}^R$ are the recovery stress fields, which will be defined in the next section, in the FEM-/ES-FEM-T3 models, respectively.

Note: the recovery-based error estimators in L2-norm only differs from those in energy norm by the weighting coefficient D.

4.2.6.2 Recovery Stress Field in FEM-T3 and ES-FEM-T3 Models.

A recovery stress field denoted as $\tilde{\sigma}^R$ and $\bar{\sigma}^R$ for the FEM-/ES-FEM-T3 models, respectively, is generated by using the nodal stress values $\tilde{\sigma}(1, 2, 3)$ and $\bar{\sigma}(1, 2, 3)$ of 1-st, 2-nd, 3-rd nodes of element. This recovery stress field is continuous on the whole problem domain and proved to fast converge to exact solutions for a very fine mesh. Therefore, it can be used as a "reference" solution for computing the error of the current model then errors indicators for adaptive analysis.

For the triangle mesh (three-node element) in the FEM-/ES-FEM-T3 models, the recovery stress field in each triangular element is interpolated by nodal stresses of that element as:

$$\tilde{\sigma}^R = \sum_{i=1}^{n_n^e} N_i(x,y)\tilde{\sigma}^R(i) \quad \text{(FEM-T3)} \qquad (4.9a)$$

$$\bar{\sigma}^R = \sum_{i=1}^{n_n^e} N_i(x,y)\bar{\sigma}^R(i) \quad \text{(ES-FEM-T3)} \qquad (4.9b)$$

where n_n^e denotes the number of nodes in an element, $n_n^e = 3$ in a triangle mesh, N_i (x, y) (i=1,2,3); N_i contains shape functions of the corresponding nodes. (these shape functions are similar to the conventional FEM-T3), $\tilde{\sigma}^R(i)$ is the vector containing the nodal stress components at the i-th (i=1,2,3) node of the element resulted from the FEM-T3, $\bar{\sigma}^R(i)$ contains the nodal stresses at the i-th (i=1,2,3) node of the element resulted from the ES-FEM-T3.

4.2.6.3 Computation of Stress at Nodes in FEM-T3 and ES-FEM-T3.

The nodal stresses $\tilde{\sigma}^R(i)$ and $\bar{\sigma}^R(i)$ can be obtained through the simple nodal averaging technique from the FEM-/ES-FEM-T3, respectively. This technique is well-

known as the first-order recovery stress first proposed by (Cook, Malkus, Plesha, & Witt, 1974) and recently applied by (Alberty, Carstensen, Funken, & Klose, 2002)

a) FEM-T3 model.

In the triangle mesh, the nodal stresses $\tilde{\sigma}(i)$ are the mean value of the stresses on the corresponding patch which includes elements surrounding and sharing that node as illustrated in Fig. 4.4 a). The area-weighted averaged stress formulation:

$$\tilde{\sigma}^R(i) = \frac{1}{A_i^{ne}} \sum_{j=1}^{n_e^i} \tilde{\sigma}_j(x_c) A_j \tag{4.10}$$

where n_e^i denotes the number of triangle elements Ω_j around the i-th node, $A_i^{ne} = \sum_{j=1}^{n_e^i} A_j$ is the total area of all the elements sharing i-th node, A_j denotes the area of the j-th element sharing the i-th node, $\tilde{\sigma}_j(x_c)$ is the compatible stress specified at the centroid of the j-th element (also that element stress in T3 mesh)

a) The elements used to calculate nodal stress j in the FEM-T3

b) The SDs used to calculate nodal stress j in the ES-FEM-T3

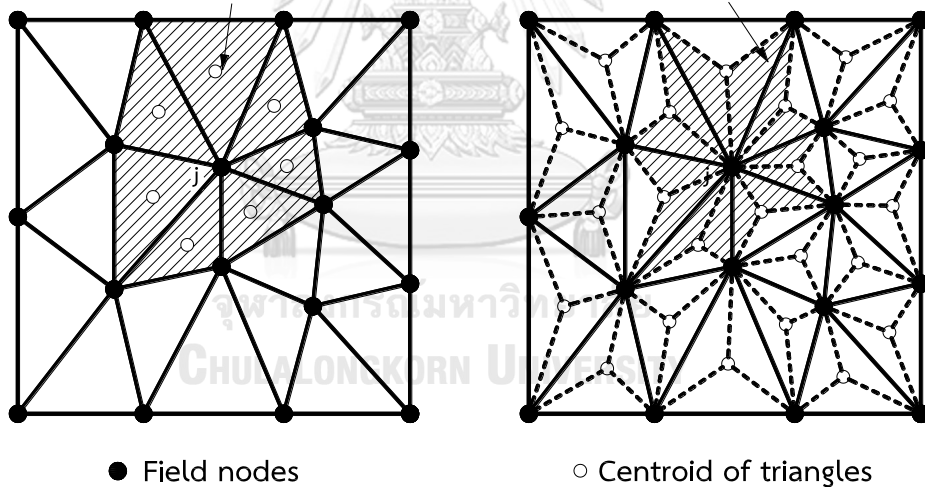● Field nodes   ○ Centroid of triangles

Figure 4.4 The elements/SDs used to calculate the nodal stresses (or strain) in the FEM-/ES-FEM-T3

b) ES-FEM-T3 model.

In a similar way as in FEM-T3, the nodal stress $\bar{\sigma}^R(i)$ is the area-weighted averaged values of smoothed stresses from SDs surrounding and sharing that node as illustrated in Fig. 4.4 b) for ES-FEM-T3.

$$\bar{\sigma}^R(i) = \frac{1}{A_i^{ns}} \sum_{k=1}^{n_s^i} \bar{\sigma}_k A_k \tag{4.11}$$

where n_s^i denotes the number of smoothing domains Ω_k around the i-th node,

$A_i^{ns} = \sum\limits_{k=1}^{n_s^i} A_k$ is the total area of all the SDs sharing the i-th node, A_k denotes the

area of the k-th SD sharing the i-th node, $\bar{\sigma}_k$ is the smoothing stress of SD Ω_k

4.2.6.4 Implementation of Recovery-Based Error Estimators in L2-Norm Using Scalar Von Mises Stress Function for FEM-T3 and ES-FEM-T3

A) Error Estimator Based on von Mises Stress Function

In elasticity theorem, the von Mises stress is proportional to the square root of the second invariant of the deviatoric stress tensor. Therefore, the recovery-based error estimator in L2-norm obeying the von Mises stress function obviously relates to the error from the element distortion energy. We have the element error indicators in L2-norm based on von Mises stress function as follows:

$$\eta_I = \left\| \tilde{\sigma}_v - \tilde{\sigma}_v^R \right\|_{L^2(\Omega_I)} = \left[\int\limits_{\Omega_I} \left(\tilde{\sigma}_v - \tilde{\sigma}_v^R \right)^T \left(\tilde{\sigma}_v - \tilde{\sigma}_v^R \right) d\Omega \right]^{1/2} \quad \text{(FEM-T3)} \qquad (4.12a)$$

$$\eta_I = \left\| \bar{\sigma}_v - \bar{\sigma}_v^R \right\|_{L^2(\Omega_I)} = \left[\int\limits_{\Omega_I} \left(\bar{\sigma}_v - \bar{\sigma}_v^R \right)^T \left(\bar{\sigma}_v - \bar{\sigma}_v^R \right) d\Omega \right]^{1/2} \quad \text{(ES-FEM-T3)} \quad (4.12b)$$

Note that:

(1) The above two Equations are nearly the same as Eqs. 4.8a, b) except replacing all stress tensors by the corresponding scalar von Mises stress of the compatible stress field in the FEM-T3 and smoothed stress field in the ES-FEM-T3.

where $\tilde{\sigma}_v$ and $\bar{\sigma}_v$ denote the numerical solutions obtained in the FEM-/ES-FEM-T3, respectively.

(2) Scalar von Mises stress field can be obtained from their corresponding stress fields.

(3) The integration in Eqs. 4.12a, b) which is the deviation between the C^0/C^{-1} continuous numerical stress field $(\tilde{\sigma}_v / \bar{\sigma}_v)$ and a higher order C^1/C^1 continuous recovery stress field $(\tilde{\sigma}_v^R / \bar{\sigma}_v^R)$ over a 2D triangle element in the FEM-/ES-FEM-T3, respectively. In the standard FEM-T3 model, the stress (or strain) is continuous in each element, while the smoothed stress (or strain) is not continuous inside elements using the model of ES-FEM-T3. It appears to be constant and discontinuous at the boundaries of SDs. The error computed by the integration of the deviation between C^-

[1] continuous numerical stress field $(\bar{\sigma}_v)$ and two higher order C[1] continuous recovery stress field $(\bar{\sigma}_v^R)$ over each triangle element becomes more complicated in the ES-FEM-T3 model. So a simple formulation will be proposed to exactly calculate these recovery-based posteriori error indicators both in the FEM-/ES-FEM-T3.

B) Implementation of Formulation for Recovery-Based Error Estimators using Scalar von Mises Stress Function.

B1) For FEM-T3: Substituting Eq. (4.19a) into Eq. (4.12a), adopting the scalar von Mises stress function, the recovery-based error indicator of the l-th triangle element in the domain:

$$\eta_l^2 = \| \tilde{\sigma}_v - \tilde{\sigma}_v^R \|_{L^2(\Omega_l)}^2 = \| \tilde{\sigma}_v - \sum_{i=1}^{3} N_i(x,y)\tilde{\sigma}_v^R(i) \|_{L^2(\Omega_l)}^2 \tag{4.14}$$

In the FEM-T3 model, the scalar von Mises stress $\tilde{\sigma}_v$ is constant inside each element Ω_l. Then, we have the stress intensity at node i (= 1, 2, 3) equals:

$$\tilde{\sigma}_v = \tilde{\sigma}_v(i) = \tilde{\sigma}_v(1) = \tilde{\sigma}_v(2) = \tilde{\sigma}_v(3) \tag{4.14}$$

The partition of unity property of the shape function, Eq. (2.13), as follows:

$$\sum_{i=1}^{3} N_i(x,y) = 1 \tag{4.15}$$

From Eqs. (4.14) & (4.15), Eq. (4.13) is rewrited by:

$$\eta_l^2 = \| \tilde{\sigma}_v - \tilde{\sigma}_v^R \|_{L^2(\Omega_l)}^2 = \| \sum_{i=1}^{3} N_i(x,y)(\tilde{\sigma}_v(i) - \tilde{\sigma}_v^R(i)) \|_{L^2(\Omega_l)}^2 \tag{4.16}$$

Let $\tilde{r}_{l,i} = \tilde{\sigma}_v(i) - \tilde{\sigma}_v^R(i)$ is the deviation between numerical von Mises stress intensity and recovery nodal von Mises stress at the i-thnode of the l-th element in the FEM-T3 model. Then from Eq. (4.16):

$$\eta_l^2 = \| \sum_{i=1}^{3} N_i(x,y)(\tilde{\sigma}_v(i) - \tilde{\sigma}_v^R(i)) \|_{L^2(\Omega_l)}^2 = \sum_{i,j=1}^{3} \tilde{r}_{l,i}\cdot\tilde{r}_{l,j} \int_{\Omega_l} N_i(x,y)N_j(x,y)d\Omega \tag{4.17}$$

From the property of the shape function, Equation (2.13), we have:

$$\int_{\Omega_l} N_i(x,y)N_j(x,y)d\Omega = \begin{cases} A_l/6 & for\ i = j, \\ A_l/12 & for\ i \neq j. \end{cases} \tag{4.18}$$

Then we finally obtain:

$$\eta_l^2 = \sum_{i,j=1}^{3} \tilde{r}_{l,i} . \tilde{r}_{l,j} \int_{\Omega_l} N_i(x,y) N_j(x,y) d\Omega \tag{4.19}$$

$$= (\tilde{r}_{l,1}^2 + \tilde{r}_{l,2}^2 + \tilde{r}_{l,3}^2 + \tilde{r}_{l,1}.\tilde{r}_{l,2} + \tilde{r}_{l,1}.\tilde{r}_{l,3} + \tilde{r}_{l,2}.\tilde{r}_{l,3}).(A_l / 6)$$

whenever $\tilde{\sigma}_v(i); \tilde{\sigma}_v^R(i)$ are available at all field nodes in the domain, the recovery-based error indicator of the l-th triangle element in the domain and the total recovery-based error indicator in the FEM-T3 model can be computed easily using Eq. (4.19)

B2) For ES-FEM-T3: Similarly, the recovery-based error indicator of the l-th triangle element in the domain can be obtained in ES-FEM-T3 model as follows:

$$\eta_l^2 = || \bar{\sigma}_v - \bar{\sigma}_v^R ||_{L^2(\Omega_l)}^2 = || \bar{\sigma}_v - \sum_{i=1}^{3} N_i(x,y) \bar{\sigma}_v^R(i) ||_{L^2(\Omega_l)}^2 \tag{4.20}$$

The scalar von Mises stress $\bar{\sigma}_v$, however, is discontinuous at the boundaries of SDs inside each element Ω_l in the ES-FEM-T3 model. The smoothed stresses in ES-FEM-T3 will constant in each smoothing domain meaning that, inside each triangle element, there will be three sub-elements with constant smoothed stress or smoothed von Mises stress as in Fig. 4.5. Therefore, the recovery-based error indicator will be computed based on the summation of errors from three sub-elements, we have:

$$\eta_l^2 = || \bar{\sigma}_v - \sum_{i=1}^{3} N_i(x,y) \bar{\sigma}_v^R(i) ||_{L^2(\Omega_l)}^2$$

$$= \sum_{q=1}^{3} || \bar{\sigma}_{v,q} - \sum_{i=1}^{3} N_{i,q}(x,y) \bar{\sigma}_{v,q}^R(i) ||_{L^2(\Omega_{l,q})}^2 \tag{4.21}$$

where $\Omega_{l,q}$ is the q-th sub-element of the l-th element, $\bar{\sigma}_{v,q}^R(i)$ is the recovery von Mises stress at the i-th node of the q-th sub-element. It is available for the 1-st and 2-nd node (field nodes) of all sub-element such as C, A in the domain $\Omega_{ABC,1} = \Delta CAI$ as in Fig. 4.5.
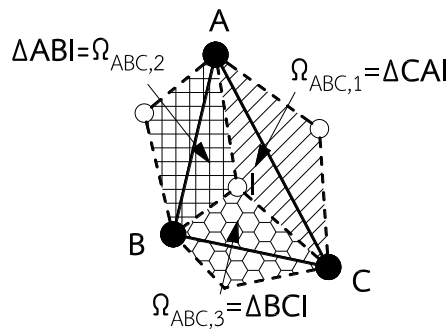

Figure 4.5 Sub-elements of a triangle element from three smoothing domains

Note: the centroid of the element will be the 3-rd node in each sub-element which is the point I as Fig. 4.5. Then, one needs to compute its recovery nodal stress by substituting its coordinates into the interpolation Eq. 4.9b) as follows:

$$\bar{\sigma}_{v,q}^{R}(3) = \bar{\sigma}_{v,1}^{R}(3) = \bar{\sigma}_{v,2}^{R}(3) = \bar{\sigma}_{v,3}^{R}(3) = \sum_{i=1}^{3} N_i(x_C, y_C)\bar{\sigma}^{R}(i) \qquad (4.22)$$

Because the smoothed stress is constant inside each sub-element, the smoothed stress intensity at i-th node (i = 1, 2, 3) equals:

$$\bar{\sigma}_{v,q} = \bar{\sigma}_{v,q}(i) = \bar{\sigma}_{v,q}(1) = \bar{\sigma}_{v,q}(2) = \bar{\sigma}_{v,q}(3) \qquad (4.23)$$

Similarly, the partition of unity property in each sub-element reads

$$\sum_{i=1}^{3} N_{i,q}(x, y) = 1 \qquad (4.24)$$

From Eqs. (4.22), (4.23) & (4.24), Eq. (4.21) is rewrited by:

$$\eta_l^2 = \| \bar{\sigma}_v - \sum_{i=1}^{3} N_i(x, y)\bar{\sigma}_v^{R}(i) \|_{L^2(\Omega_l)}^2$$

$$= \sum_{q=1}^{3} \| \sum_{i=1}^{3} N_{i,q}(x, y)(\bar{\sigma}_{v,q}(i) - \bar{\sigma}_{v,q}^{R}(i)) \|_{L^2(\Omega_{l,q})}^2 \qquad (4.24)$$

Let $\bar{r}_{l,q,i} = \bar{\sigma}_{v,q}(i) - \bar{\sigma}_{v,q}^{R}(i)$ is the deviation between smoothed von Mises stress intensity and recovery nodal von Mises stress at an i-thnode of the q-th sub-element of element l, in ES-FEM-T3 model. Then from Eq. (4.25):

$$\eta_l^2 = \sum_{q=1}^{3} \| \sum_{i=1}^{3} N_{i,q}(x, y)(\bar{\sigma}_{v,q}(i) - \bar{\sigma}_{v,q}^{R}(i)) \|_{L^2(\Omega_{l,q})}^2$$

$$= \sum_{q=1}^{3} \left[\sum_{i,j=1}^{3} \bar{r}_{l,q,i} \cdot \bar{r}_{l,q,j} \int_{\Omega_{l,q}} N_{i,q}(x, y)N_{j,q}(x, y)d\Omega \right] \qquad (4.26)$$

Similarly, from the property of the shape function for each sub-element, we have:

$$\int_{\Omega_{l,q}} N_{i,q}(x, y)N_{j,q}(x, y)d\Omega = \begin{cases} A_{l,q}/6 = A_l/18 & \text{for } i = j, \\ A_{l,q}/12 = A_l/36 & \text{for } i \neq j. \end{cases} \qquad (4.27)$$

where $A_{l,q}$ denotes the area of the q-th sub-element of the element l, which equals one-third of the area of the element l. For example, $A_{CAI} = A_{ABI} = A_{BCI} = (1/3)A_{ABC}$ as in Fig. 4.5. We finally obtain:

$$\eta_l^2 = \sum_{q=1}^{3}\left[\sum_{i,j=1}^{3}\overline{r}_{l,q,i}.\overline{r}_{l,q,i}\int_{\Omega_{l,q}}N_{i,q}(x,y)N_{j,q}(x,y)d\Omega\right]$$

(4.28)

$$= \sum_{q=1}^{3}\left[(\overline{r}_{l,q,1}^2 + \overline{r}_{l,q,2}^2 + \overline{r}_{l,q,3}^2 + \overline{r}_{l,q,1}.\overline{r}_{l,q,2} + \overline{r}_{l,q,1}.\overline{r}_{l,q,3} + \overline{r}_{l,q,2}.r_{l,q,3}).(A_l/18)\right]$$

whenever $\bar{\sigma}_{v,q}(i);\bar{\sigma}_{v,q}^{R}(i)$ are available at all field nodes and at the centroid of all triangle elements in the domain, the recovery-based error indicator of the l-th triangle element in the domain and the total recovery-based error indicator in the ES-FEM-T3 can be computed easily using Eq. (4.28)

4.3 Enhancing Computing Efficiency by Vectorization Language and Built-In Functions

Some ideals was first introduced by (Getreuer, 2006) for researchers using MATLAB language for programming. Recently, the successful application of those advance techniques into numerical method, specially FEM-T3, has been shown by (Rahman & Valdman, 2013); (Funken, Praetorius, & Wissgott, 2011); (Cuvelier, Japhet, & Scarella, 2016). Therefore, the vectorization for our code in each adaptive loop is essential for optimizing the runtime as well as storage of the code. In this work, we will apply vectorization for some steps. We will perform in the sense of eliminating as many as possible for-loops in the same adaptive scheme for both for the FEM-/ES-FEM-T3.

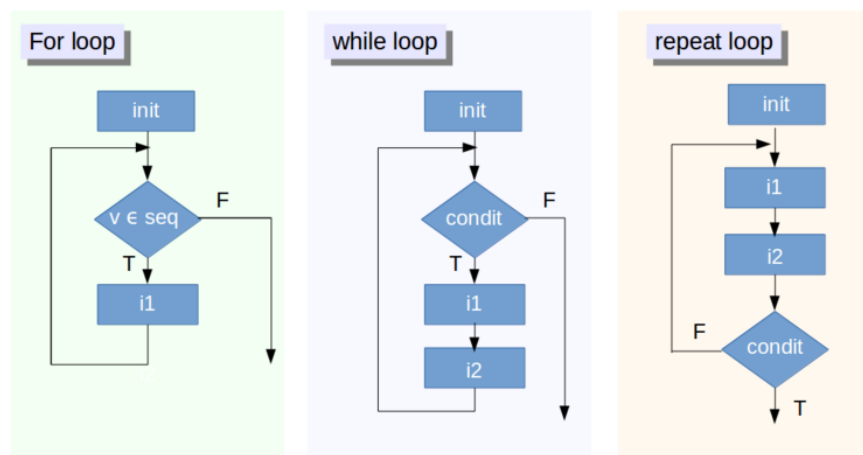### 4.3.1 Loops in Classical Algorithm

Figure 4.6 Loops in MATLAB

As mentioned above, the algorithms that use these loops for computing a matrix or constructing a new matrix cost a lot of work to do and it will repeat every calculation loop. In addition, many adaptive procedures often have loops inside loops that will require a huge amount of runtime and storage.

4.3.2 Matrix, Logical Array Operations and Ordering, Setting, and Counting Operations.

Built-in MATLAB functions help to implement the vectorization and make a combined set of operations generally classified as follows:

(1) Matrix Operations

(2) Logical Array Operations

(3) Ordering, Setting, and Counting Operations.

Functions that is widely used in vectorization as in Table 5.1

Table 5.1 Functions commonly used in vectorization	
Function	**Description**
accumarray	accumulating elements of a vector using the subscripts
all	Determine whether all array elements are nonzero or true
any	Determine whether any array elements are nonzero
cumsum	Cumulative sum of
diff	Differences and Approximate Derivatives
find	Find indices and values of nonzero elements
logical	Convert numeric values to logicals
mat2vec	Convert a matrix (nxm) into a vector
repmat	Repeat copy of array
reshape	Reshape array
sparse	Construct a sparse matrix based on row, column index and values
setdiff	Find elements different from 2 matrix
sort	Sort array elements

sum	Summation of array elements
unique	Find unique elements
vec2mat	Convert a vector into a matrix (nxm)

4.4 Illustrative Examples.

The two problems, from a number of which successfully solved, are double-edge notched specimen and Prandtl's punch (Tangaramvong, Tin‑Loi, & Song, 2012) and. They serve as benchmarks for any analysis methods developed to provide solutions of the challenging problems under the presence of stress singularity and discontinuity field. Processing such problems often require excessive computing resources. Robust numerical method is thus necessary. The reference values is extracted from (Tangaramvong et al., 2012) without considering the plastic response of the problems. The proposed models were encoded within a MATLAB environment.

4.4.1 Example 1: Double-Edge Notched Specimen

A plane strain double-edge notched specimen in Fig. 4.7a) was subjected to the total uniform lateral load of 1.44. The material properties of $E = 70$, $v = 0.3$ and $t = 1$ were adopted. Due to symmetry in both x- and y-axis, a quarter of the specimen without undue loss of accuracy was analyzed. The initial characteristic ES-FEM-T3 with 150 elements is displayed in Fig. 4.7b).

The proposed ES-FEM-T3 analysis approach with uniform model construction was successfully performed. The relations between computed lateral displacements v, corresponding degrees of freedoms (DOFs) and CPU times are displayed in the two Figs. 4.8 and 4.9, respectively. The responded displacements v shown in the similar figures were also obtained by some standard isoparametric FEMs, namely FEM-T3 and FEM-Q4.

All analysis methods converged to the reference values as the discrete models were sufficiently refined. The ES-FEM-T3 present the more efficient and robust elastic analysis scheme as compared to the other FEM-T3 and FEM-Q4 approaches. Figs. 4.8 and 4.9 show the displacement solutions computed by ES-FEM-T3 converged with less

computing efforts (i.e. numbers of elements and numbers of DOFs) as compared to FEM-T3 and FEM-Q4.
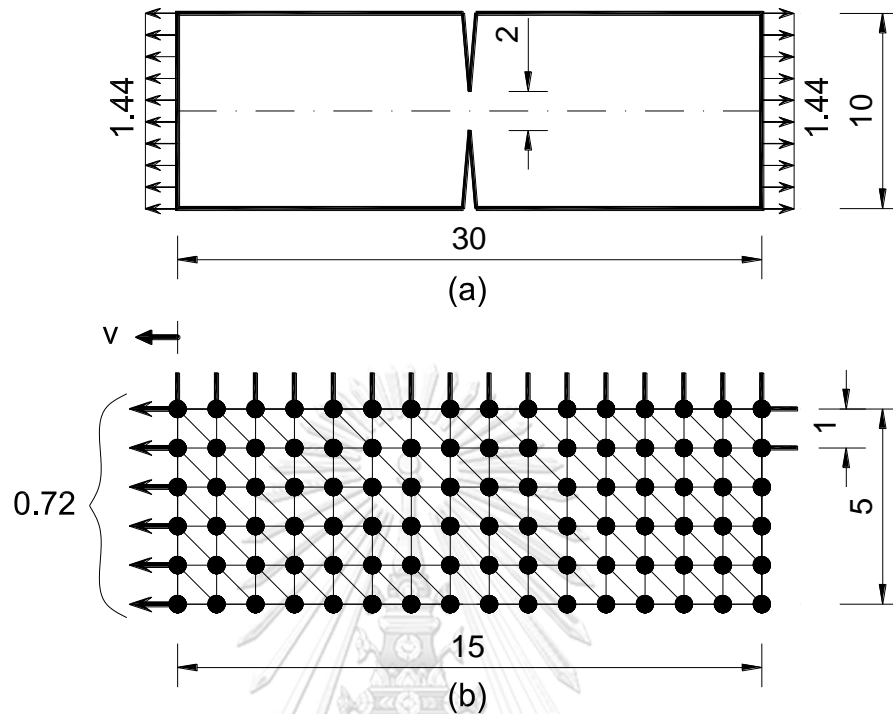

(a)

(b)

Figure 4.7 Example 1: Double-edge notched problem (a) geometry and loading (b) ES-FEM-T3 model of a triangle mesh (the thick solid lines denote nodal restrained directions).
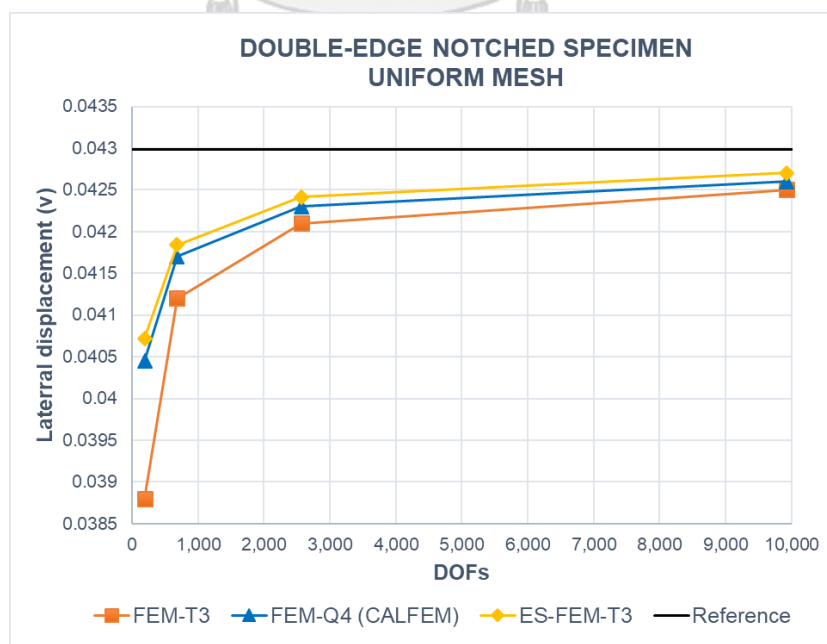

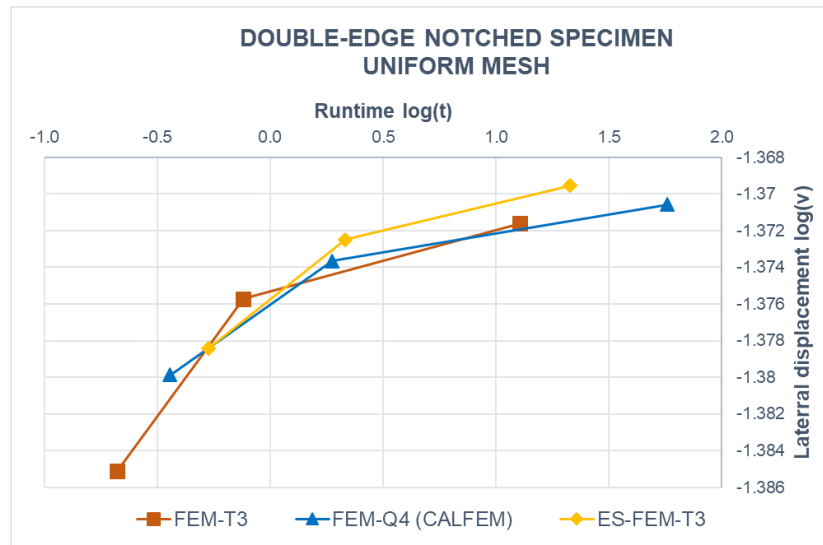Figure 4.8 Example 1: Convergence of horizontal displacement results.

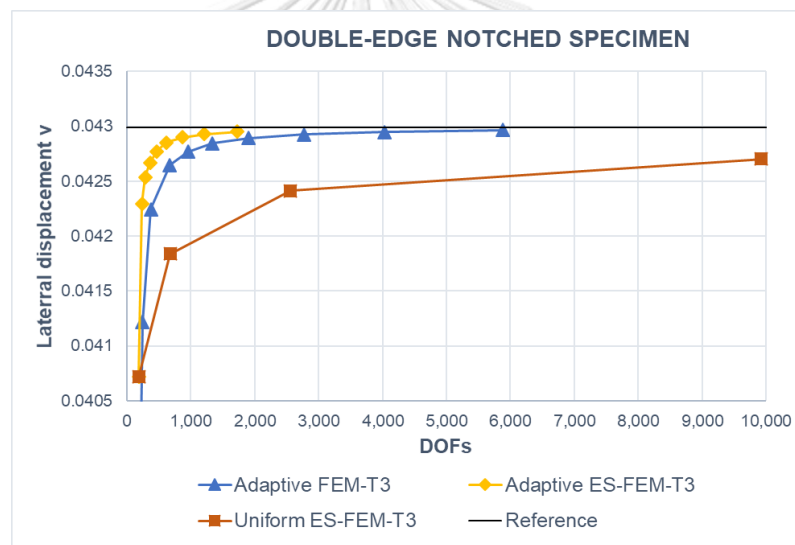Figure 4.9 Example 1: CPU times run for various FEM models.

Figure 4.10 Example 1: Convergence of lateral displacement results for various
automatic adaptive mesh algorithms.

Moreover, the ES-FEM-T3 incorporated the automatic adaptive scheme adopting recovery-based strain error functions. The lateral displacements v and strain energy responses (displayed in Figs. 4.10 and 4.11, respectively) were successfully computed for various mesh refinements, and compared with those in other standard FEM models adopting the same adaptive algorithm.
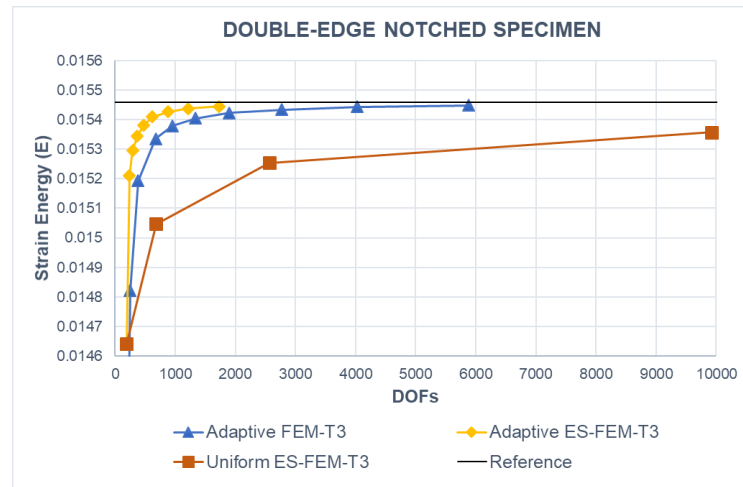
Figure 4.11 Example 1: Convergence of strain energy results for various automatic
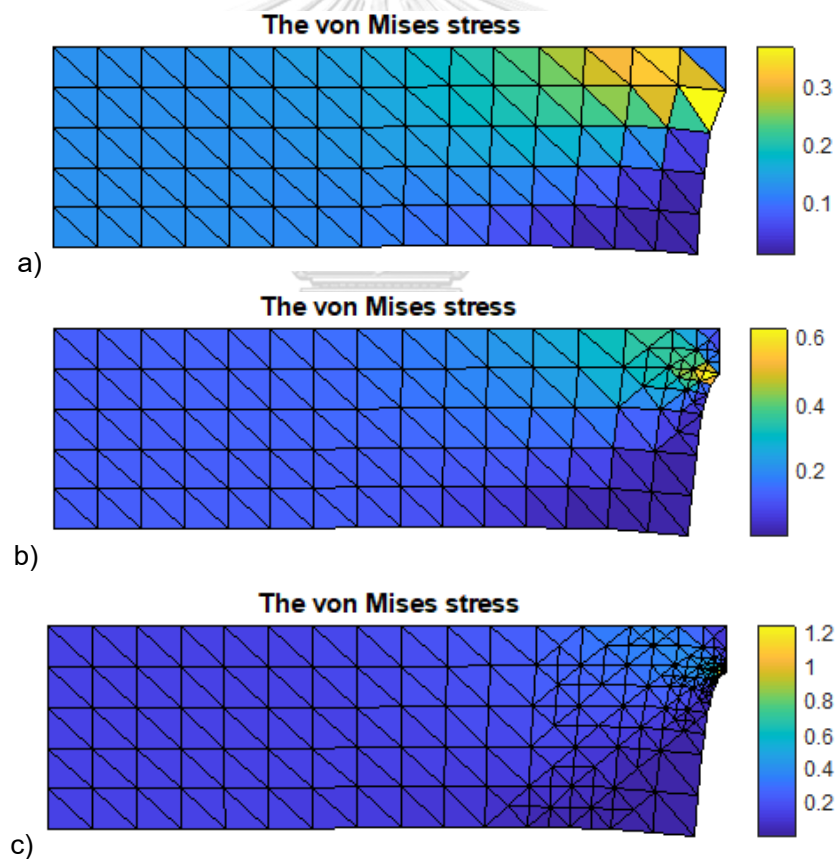
adaptive mesh algorithms

Figure 4.12 Example 1: Automatic adaptive meshes with corresponding von Mises

stress distributions. (a) 150 elements – relative error 14.16% (b) 199 elements –

relative error 8.89% (c) 360 elements – relative error 5.78%

As shown in these Figs. 4.10 and 4.11, the analysis solutions accurately converged to the reference values with minimum numbers of DOFs. The mesh discretized patterns in Fig. 4.12 as expected progressively refined over the concentrated stress singularity and discontinuity areas.

4.4.2 Example 2: Prandtl's Punch

The second example considers a well-known Prandtl's punch problem with flexible foundation drawn in Fig. 4.13a). The footing was modeled as a total uniformly distributed loads of 10. The material properties employed were: $E = 10^4$, $v = 0.25$ and $t = 1$. In view of symmetry in both geometry and loading configurations, only half of the structure is modeled in plane strain. The characteristic discrete structural model in Fig. 4.13b) contains 256 three-node elements.
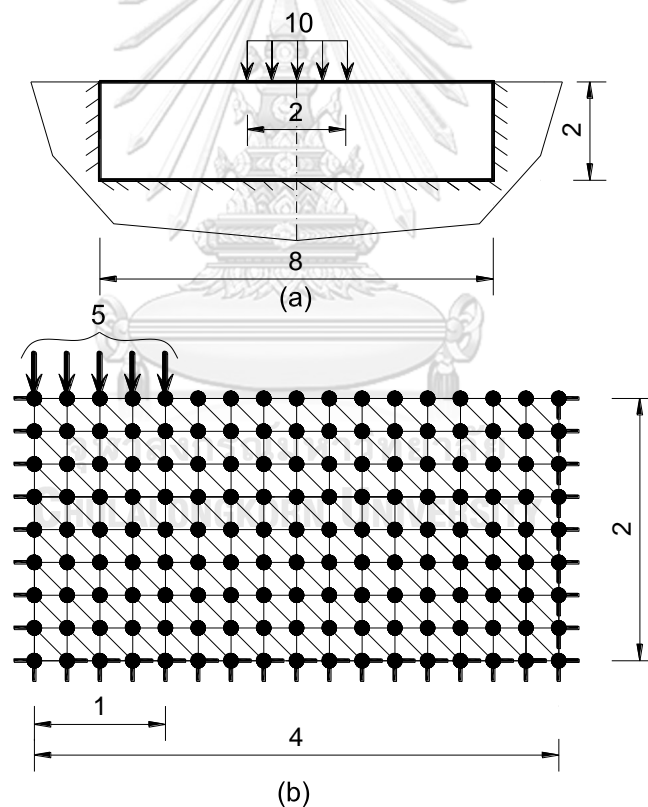

Figure 4.13 Example 2: Prandtl's punch (a) geometry and loading, (b) ES-FEM-T3 model of triangle mesh, (thick solid lines denote nodal restrained directions)
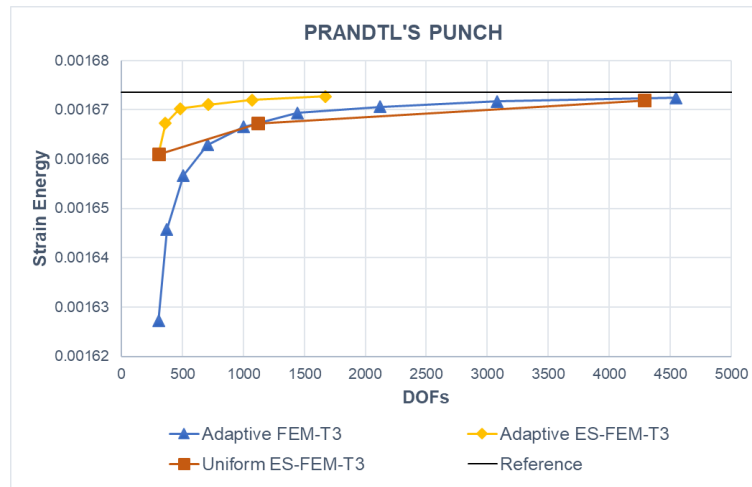
Figure 4.14 Example 2: Convergence of strain energy results from various analysis methods.

The proposed automatic adaptive ES-FEM-T3 analysis approach was successfully processed to obtain elastic strain energy response solutions. The analysis results computed are plotted with their associated DOFs in Fig. 4.14, where those of some other standard FEMs, namely FEM-T3 with mesh adaptive scheme and ES-FEM-T3 with uniform mesh refinement. It is clear that all methods produce the solutions converged to the reference value with the sufficient fine numbers of discrete elements.
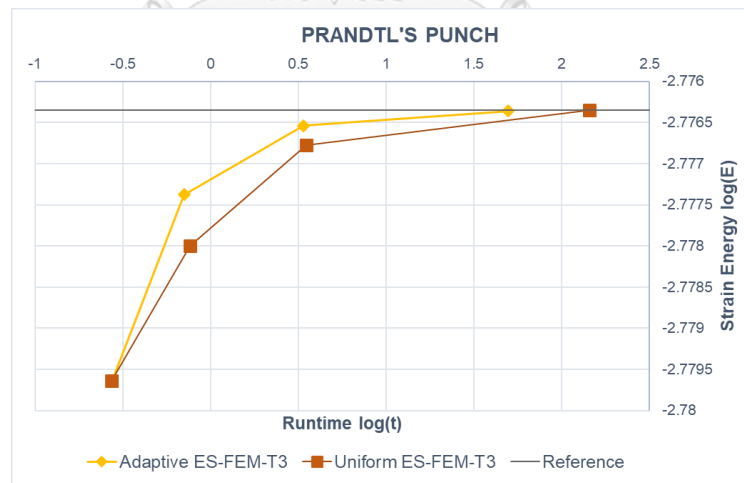

Figure 4.15 Example 2: Convergence rate of runtime versus strain energy between uniform and adaptive ES-FEM-T3 models

Once again, the proposed automatic adaptive ES-FEM-T3 approach provided the fast-converged strain energy solutions as compared to ES-FEM-T3 with uniform mesh refinement. The computing times as required for successfully converging the results by

automatic mesh adaptive recovery-based strain algorithm, as displayed in Fig. 4.15, were less than those from standard uniform mesh refining technique. The von Mises stress results corresponding to automatically adaptive meshes are depicted in Fig. 4.16. It illustrates the mesh refinements localizing over strong stress discontinuity areas.
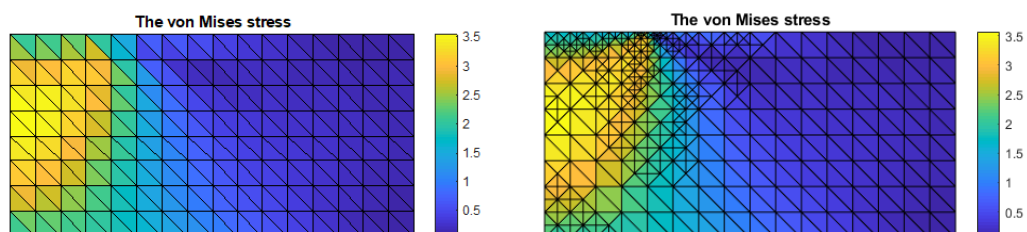
(a) 256 elements – relative error 7%   (b) 637 elements – relative error 4.27%

(c) 1565 elements – relative error 2.73%

Figure 4.16 Example 2: Automatic adaptive meshes with corresponding von Mises stress distributions.

Remarks:

The novel ES-FEM-T3 approach with an automatic AMR algorithm has been presented to efficiently and accurately provide the response solution of elastic structures. The automatic AMR adopted the newest vertex bisection algorithm with recovery-based error function. A number of numerical benchmarks (including both benchmarks and practical in-plane structures) were successfully solved using the proposed analysis scheme. Two of which are given in this paper. These illustrate robustness of the proposed analysis method, in which the adaptive ES-FEM-T3 approach provided the fast convergence of elastic response solutions as compared to conventional FEMs. The computed results agreed well with all reference values, and thus evidenced the computational advantages in yielding the close-to-exact solutions for modest computing resources.

CHAPTER 5 AUTOMATIC ADAPTIVE SINGULAR ES-FEM-T3

5.1 Introduction

The numerical solutions from Chapter 4 illustrate the robustness of the proposed analysis scheme with fast convergence of the adaptive ES-FEM-T3 against the standard FEMs. These challenging problems are successfully captured the presence of stress singularity or discontinuity field by a sufficient fine mesh around the singularity point. However, if we further zoom in a local area of triangle elements surrounding the crack-tip point, a linearly approximate interpolation will not properly represent for the singular solution fields. Therefore, in this Chapter, another layer of singular elements around the crack-tip point is combined with the remaining area of unchanged three-node triangle element for sovling the cracking problems.

Adopting the recovery-based error function in energy norm for a sES-FEM-T3-5, (Hung Nguyen-Xuan et al., 2013) predicted accurately the singular stress field of arbitrary order around re-entrant corners (free-free BC on angle faces).

The proposed adaptive mesh implementation adopted a similar recovery-based error indicator, but in L2-norm, in singular ES-FEM-T3 model is conducted in this chapter for problems of having angular corners under some other BCs. Two numerical examples about cracking problems, one is the same Example 1 of double-edge notched specimen in previous Chapter and another is the concrete dam with a crack in the footing, both of them in the plane strain condition.

5.2 Adaptive Algorithm Implementation

The adaptive algorithm adopted in the singular ES-FEM-T3 is similar as that in Section 4.2. For regular three-node triangle elements which are not directly related to the crack-tip, the adaptive procedure is exactly the same as three-node elements in ES-FEM-T3. Therefore, we will not repeatedly this procedure in-detail in this Chapter. The following parts propose an error indicator that is suitable and properly implemented into the proposed mesh adaptation for the singular ES-FEM-T3 for singular problems.

5.2.1 Error Assessment in Singular ES-FEM-T3.

5.2.1.1 Global Recovery-Based Error Estimator in L2 and Energy Norm.

In the singular ES-FEM-T3, the recovery-based error estimator in L2-norm is performed based on both regular three-node triangle elements and five-node singular triangle elements.

The total ZZ-type error estimator

$$\eta_Z = \left(\sum_{l=1}^{N_{e-3}} \eta_l^2 + \sum_{l=1}^{N_{e-5}} \eta_{s,l}^2 \right)^{1/2} \tag{5.1}$$

where $\eta_l, \eta_{s,l}$ is recovery-based error indicator of the l-th regular and singular triangle element in the singular ES-FEM-T3, $\eta_{s,l}$ in L2-norm reads

$$\eta_{s,l} = \left\| \bar{\sigma}_s - \bar{\sigma}_s^R \right\|_{L^2(\Omega_l)} = \left[\int_{\Omega_l} \left(\bar{\sigma}_s - \bar{\sigma}_s^R \right)^T \left(\bar{\sigma}_s - \bar{\sigma}_s^R \right) d\Omega \right]^{1/2} \tag{5.2}$$

where $\bar{\sigma}_s$ is the numerical solution for stress of singular elements and $\bar{\sigma}_s^R$ is the recovery stress field of singular elements, which will be defined in the next section for singular ES-FEM-T3 model.

In this singular model, the numerical solution $\bar{\sigma}_s$ of the singular smoothing domains, e.g. 1-A2-A1-2-B1-B2-1 in Fig. 5.1, has two different values for two layers, namely 1-A2-4-B2-1 and A2-A1-2-B1-B2-4-A2, respectively. In order to compute the error in Eq. (5.2), we apply the simple area-weighted averaging technique to obtain the unique solution (stress or strain) in each singular smoothing domain by

$$\bar{B}_i = \frac{1}{A_k^s} \sum_{a=1}^{2} A_k^{s,a} \bar{B}_i^a \tag{5.3}$$

where $\bar{B}_i^a, A_k^{s,a}$ denote the smoothed strain–displacement matrix and areas of the a-th layer of the singular smoothing domains Ω_k^s, respectively, $A_k^s = \sum_{a=1}^{2} A_k^{s,a}$ is the area of the singular smoothing domains Ω_k^s.

As shown on the Fig. 5.1, we have: $\bar{B}_i = \dfrac{A_k^{s,1} \bar{B}_i^1 + A_k^{s,2} \bar{B}_i^2}{A_k^s} \tag{5.4}$
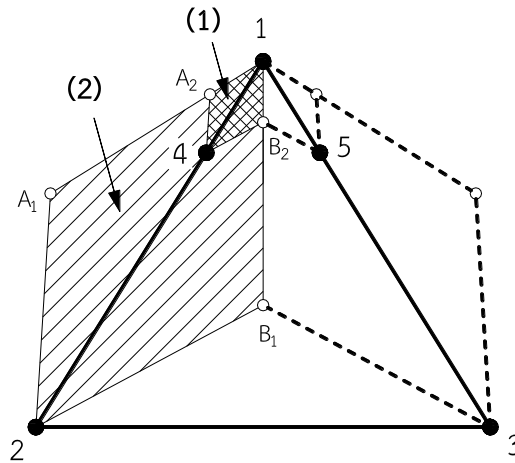
Figure 5.1. Averaging the smoothed stress for singular smoothing domains.

5.2.1.2 Recovery Stress Field in Singular ES-FEM-T3.

A recovery stress field, $\bar{\sigma}_s^R$, is constructed from the smoothed nodal stresses obtained from the singular ES-FEM-T3 together with the linear shape functions of the standard constant strain element.

$$\bar{\sigma}_s^R = \sum_{i=1}^{n_n^e} N_i(x,y)\bar{\sigma}_s^R(i) \tag{5.5}$$

where $n_n^e = 3$ denote the number of original field nodes of an singular triangle element, $N_i(x, y)$ (i=1,2,3) contains shape functions of the corresponding nodes. (these shape functions are the same as in the conventional FEM-T3), $\bar{\sigma}_s^R(i)$ contains the nodal stresses at the i-th (i=1,2,3) node of the singular element in singular ES-FEM-T3 and is presented in the next section.

5.2.1.3 Evaluation of Stress at Nodes in Singular ES-FEM-T3.

The nodal stress $\bar{\sigma}_s^R(i)$ in singular ES-FEM-T3 is also computed using the similar simple nodal averaging technique for all nodes in the domain.

In a similar way as in ES-FEM-T3, the nodal stresses $\bar{\sigma}^R(i)$ are the area-weighted averaged values of smoothed stresses from smoothing domains (SDs) surrounding and sharing that node. Three cases corresponding to three different types of node will be conducted in this model as illustrated in Figs. 5.2 a, b and c), namely regular node, node directly connected to singular point and singular node (point), respectively.

$$\bar{\sigma}_s^R(i) = \frac{1}{A_i^{ns}} \sum_{k=1}^{n_s^i} \bar{\sigma}_{s,k} A_k \qquad (5.6)$$

where n_s^i denote the number of SDs around the i-th node, $A_i^{ns} = \sum_{k=1}^{n_s^i} A_k$ is the total area of all SDs sharing the i-th node as illustrated in Fig. 5.2, $\bar{\sigma}_{s,k}$ is the smoothed stress of smoothing domains Ω_k

For the nodes in case b, the layer of singular SDs closes the node will be considered for computing. Similarly in case c, the layer of singular SDs directly connected to the singular node is used.

a) The SDs used to calculate nodal stress far away from singular point

b) The SDs used to calculate nodal stress directly connect to singular point

c) The SDs used to calculate nodal stress at singular point

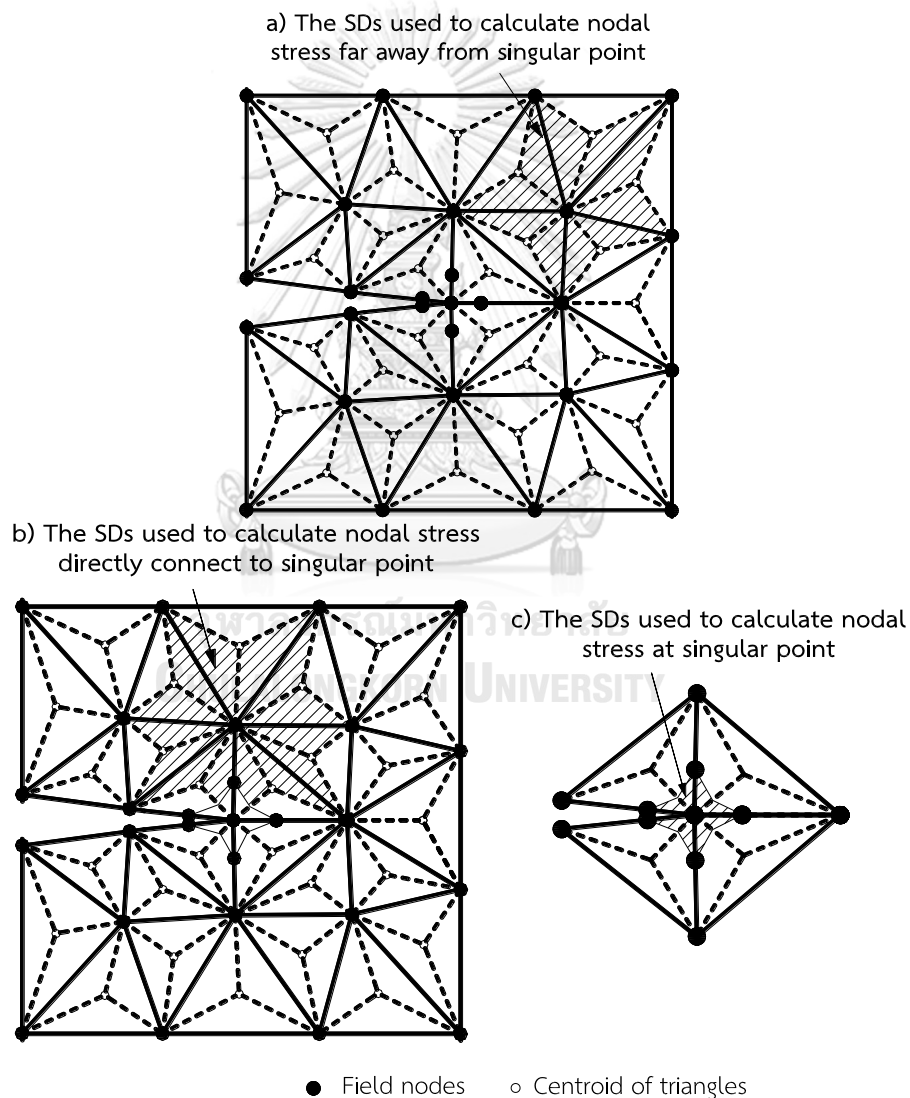● Field nodes   ○ Centroid of triangles

Figure 5.2. The sub-/SDs used to calculate the recovery nodal stresses in the singular ES-FEM-T3

5.3 Illustrate Examples

The two numerical examples related to cracking problems are used in this Chapter. One is the double-edge notched specimen in previous Chapter and another is the well-known concrete dam with a crack in the footing, both of them in the plane strain condition. The first example in linear elastic is solved again to provide a higher level of accuracy using the proposed mesh adaptation adopted a layer of singular triangular element around the crack-tip so-called adaptive singular ES-FEM-T3. Whereas the second example was introduced (Theme, 1999) for the safety assessment of the concrete gravity dam. Several numerical models, such as the bilinear mixed FEM by (Tangaramvong & Tin-Loi, 2012) or scaled boundary FEM by (Zhong, Li, Ooi, & Song, 2018), have been applied for solving the problem of crack propagation at the interfaces between a concrete dam and a rigid foundation. The density of mesh around the crack tip is expected to be finer than others. The proposed mesh adaption in the framework of the singular ES-FEM-T3 is used to provide the static-elastic responses of present structure.

5.3.1 Example 1: Double-Edge Notched Specimen

The same problem as in Section 4.4.1 is considered in this example, but using the adaptive singular ES-FEM-T3.

Compared with the results obtained from the previous Chapter, the adaptive singular ES-FEM-T3 converged with a more reasonable computing efforts (DOFs) in terms of both the lateral displacements v and strain energy solutions (displayed in Figs. 5.3 and 5.4, respectively). Moreover, either ES-FEM or FEM all provide solution towards reference values adopting the same proposed approach.
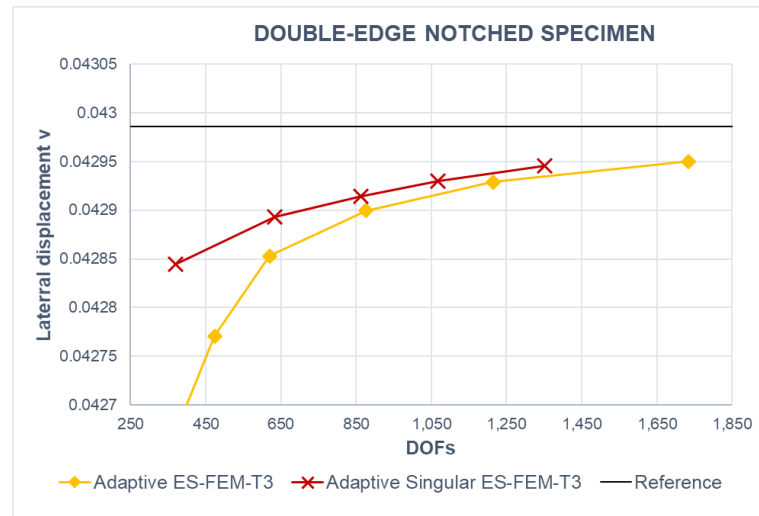
Figure 5.3 Example 1: Convergence of lateral displacement results from adaptive ES-FEM-T3 and adaptive singular ES-FEM-T3
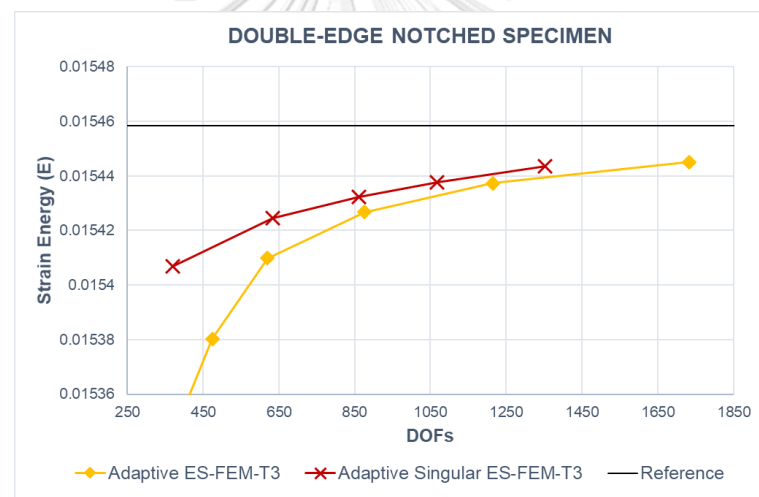
Figure 5.4 Example 1: Convergence of strain energy results from adaptive ES-FEM-T3 and adaptive singular ES-FEM-T3

Within the framework of singular ES-FEM-T3, the present adaptive mesh implementation significantly reduces the recovery-based relative error compared to the normal uniform refinement strategy. The value from adaptive singular ES-FEM-T3 navigates to the zero value, while that from uniform singular ES-FEM-T3 still stands at a very high value (e.g. less than 5% can be obtained with about 500 DOFs as shown in Fig. 5.5.
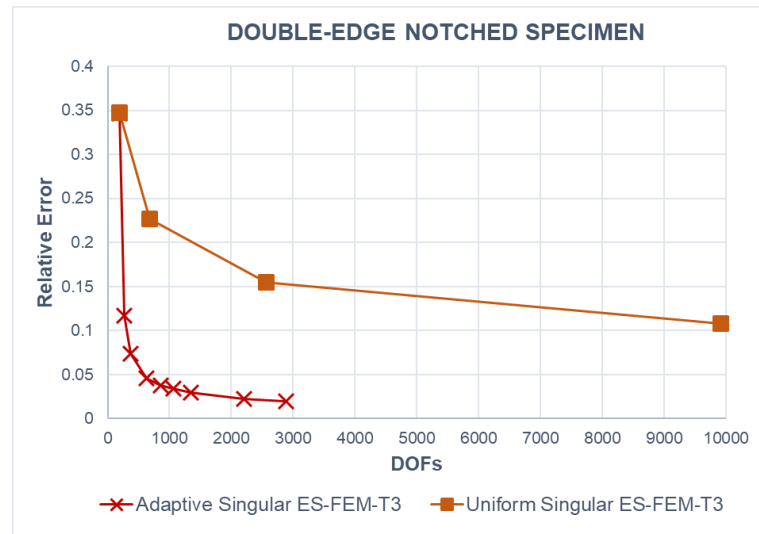
Figure 5.5 Example 1: Convergence of relative error results from adaptive singular ES-FEM-T3 and uniform singular ES-FEM-T3

5.3.2 Example 2: Concrete Gravity Dam

A concrete gravity dam (Bolzon, 2017) depicted in Fig. 5.6a) with a self-weight of 24 kN-m^{-3} was supported by a solid foundation and applied by the hydraulic pressure (water weight of 10 kN-m^{-3}) at an upstream face. The proposed analysis algorithm was performed to tra the complete responses between the overflow water level α (unit-m) and uplift v (m) at an upstream corner base. The concrete body assumed the elastic homogeneous material properties ($E = 24 \times 10^6$ kN-m^{-2} and $v = 0.15$), and the potential damaged interface Γ_c was described by the mode-I cohesive fracture, where the smooth interface was suitably discretized into the set of c contact points k. The tensile traction strength of $r_c^k = r_0 e^{-\beta \zeta^k}$ (kN) was employed with the initial capacity of $r_0 = 300$ kN-m^{-2} and the stress degradation rate of $\beta = 10^5$ (viz., immediate loosing of contact tractions at crack openings). In addition to the upstream hydraulic pressure, the two uplift load p_c^k Cases i perfect drainage ($p_c^k=0$) and Case ii imperfect drainage given by $p_c^k = p_0(1 - e^{-\rho \zeta^k})$, established along the cracked interface (i.e., $\zeta^k > 0$), where p_0 is a water pressure at the bottom face and $\rho = 33.33$ for an uplift pressure distribution.
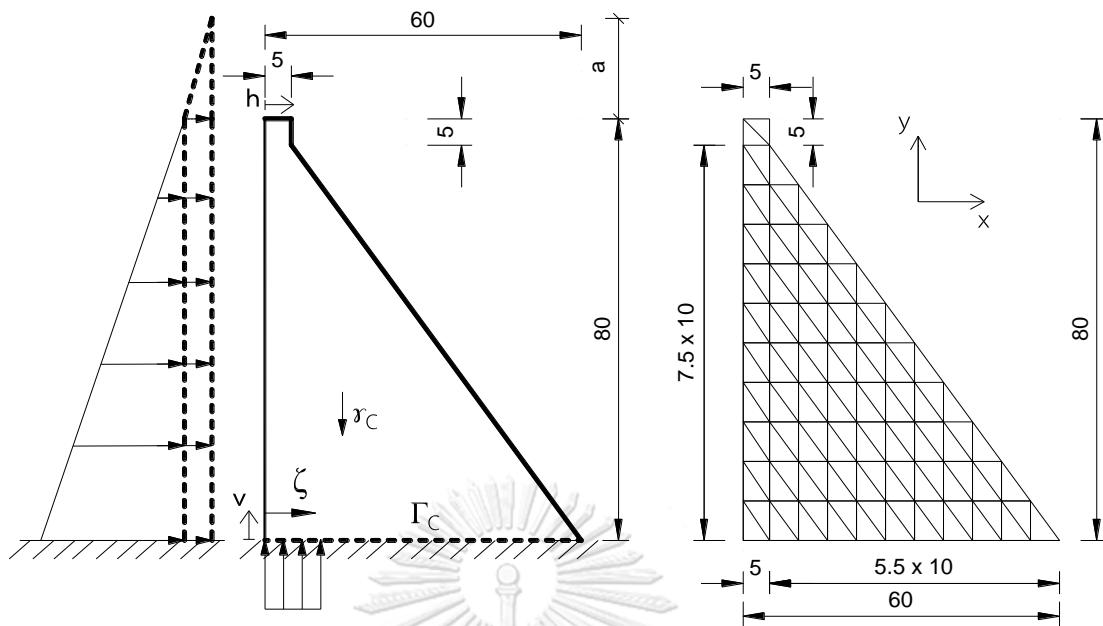
Figure 5.6 Example 2: Concrete Dam (a) geometry and loading, (b) ES-FEM model of triangle mesh

The structure was discretized as the initial characteristic three-node ES-FE model in plain strain (containing 122 elements with 158 degrees of freedom) in Fig. 5.6b). The proposed approach was successfully performed for both analysis cases under monotonic increases of $\Delta\alpha$ = 0.1 up to the predefined uplift limit of v_{limit} = 0.1 m. For the imperfect drainage Case ii, the water level increment of $\Delta\alpha$ = -0.1 was applied over the post-collapse behaviours. The resulting α - v responses for the two uplift cases were plotted in Fig. 5.7, where the maximum overflow water levels of α_{max} = 26.2 m and 12.7 m were computed for Cases i and ii, respectively. The corresponding von Mises stress distributions to the α_{max} are depicted in Figs. 5.8a) and 5.8b). In essence, these illustrate the efficiency of the automatic adaptive ES-FE constructions, namely mesh refinements following the moving crack tips along the damaged interface Γ_c and coarsern meshes after loosing of the interface tractions, and the robustness of the proposed ES-FE complementarity algorithm in providing the complete post-collapse behaviours at modest computing resources.
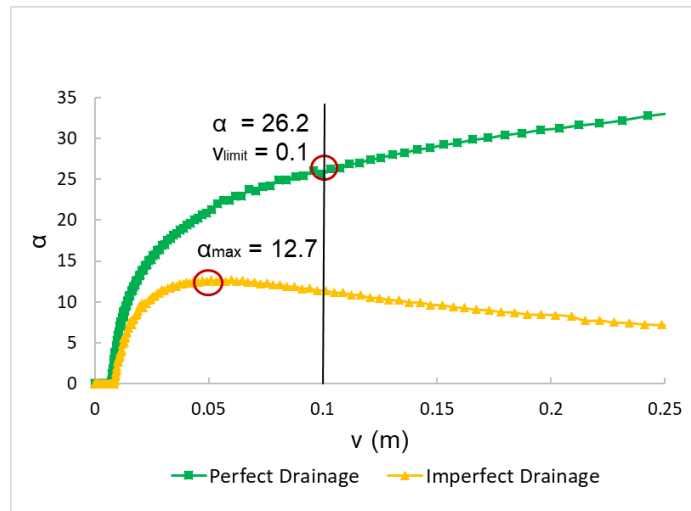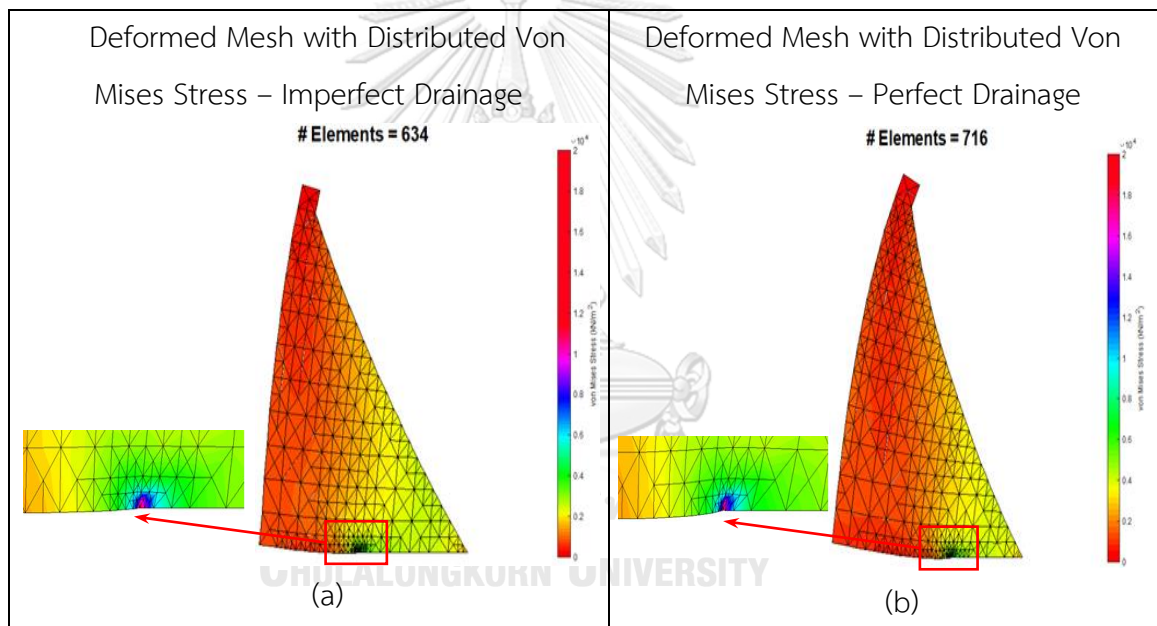
Figure 5.7 Example 2: α - v responses

Figure 5.8 Example 2: (a) von Mises stress distribution at α_{max} for an imperfect drainage case, (b) von Mises stress distribution at v_{limit} for a perfect drainage case.

CHAPTER 6 CONCLUSION AND FUTURE RESEARCH

The novel ES-FEM-T3 and singular ES-FEM-T3 approaches employed automatic AMR algorithm to efficiently and accurately provide the response solution of elastic structures. The automatic AMR adopted the newest vertex bisection algorithm and recovery-based error function in L2-norm. A number of numerical benchmarks (including both mechanics problems and practical in-plane structures) were successfully solved using the proposed analysis scheme. Three of which are given in this study. These illustrate robustness of the proposed analysis method, in which the adaptive singular ES-FEM-T3 approach provided the superconvergence of elastic response solutions as compared to the other models for crack problems and the adaptive ES-FEM-T3 approach for general discontinuity problems (e.g. discontinuity applied load). The computed results agreed well with all reference values, and thus evidenced the computational advantages in yielding the close-to-exact solutions for modest computing resources. In addition, it is clear that the refinement properly focus around the crack-tip.

The present approach has been also applied to trace the full responses of concrete gravity dam with damaged interfaces at solid foundation. The stepwise holonomic algorithm is employed to captures the post-collapse behaviours of the concrete dam under hydraulic pressures. This algorithm within the automatic adaptive ES-FEM provides the robust modelling and solution framework to capture crack propagation in fracture mechanics applications.

A nontrivial extension of the proposed analysis scheme is the applications in contact and nonlinear fracture mechanics, where the structures are severely subjected to the numerically instabilizing problems involving from stress singularity at crack tips.

REFERENCES

Ainsworth, M., Zhu, J., Craig, A., & Zienkiewicz, O. (1989). Analysis of the Zienkiewicz–Zhu a-posteriori error estimator in the finite element method. *International Journal for Numerical Methods in Engineering, 28*(9), 2161-2174.

Alberty, J., Carstensen, C., Funken, S. A., & Klose, R. (2002). Matlab implementation of the finite element method in elasticity. *Computing, 69*(3), 239-263.

Babuška, I., & Rheinboldt, W. C. (1978). A-posteriori error estimates for the finite element method. *International Journal for Numerical Methods in Engineering, 12*(10), 1597-1615.

Bolzon, G. (2017). Complementarity problems in structural engineering: an overview. *Archives of Computational Methods in Engineering, 24*(1), 23-36.

Bordas, S. P., Rabczuk, T., Hung, N.-X., Nguyen, V. P., Natarajan, S., Bog, T., & Hiep, N. V. (2010). Strain smoothing in FEM and XFEM. *Computers & structures, 88*(23-24), 1419-1443.

Chen, J. S., Wu, C. T., Yoon, S., & You, Y. (2001). A stabilized conforming nodal integration for Galerkin mesh-free methods. *International Journal for Numerical Methods in Engineering, 50*(2), 435-466.

Chen, L., Liu, G., Jiang, Y., Zeng, K., & Zhang, J. (2011). A singular edge-based smoothed finite element method (ES-FEM) for crack analyses in anisotropic media. *Engineering fracture mechanics, 78*(1), 85-109.

Chen, L., Liu, G., Nourbakhsh-Nia, N., & Zeng, K. (2010). A singular edge-based smoothed finite element method (ES-FEM) for bimaterial interface cracks. *Computational Mechanics, 45*(2-3), 109.

Chen, L., & Zhang, C. (2010). A coarsening algorithm on adaptive grids by newest vertex bisection and its applications. *Journal of Computational Mathematics*, 767-789.

Comninou, M. (1976). Stress singularity at a sharp edge in contact problems with friction. *Zeitschrift für angewandte Mathematik und Physik ZAMP, 27*(4), 493-499.

Cook, R. D., Malkus, D. S., Plesha, M. E., & Witt, R. J. (1974). *Concepts and applications of finite element analysis* (Vol. 4): Wiley New York.

Cui, X., Liu, G., Li, G., Zhang, G., & Sun, G. (2009). Analysis of elastic–plastic problems using edge-based smoothed finite element method. *International Journal of Pressure Vessels and Piping, 86*(10), 711-718.

Cuvelier, F., Japhet, C., & Scarella, G. (2016). An efficient way to assemble finite element matrices in vector languages. *BIT Numerical Mathematics, 56*(3), 833-864.

Dörfler, W. (1996). A convergent adaptive algorithm for Poisson's equation. *SIAM Journal on Numerical Analysis, 33*(3), 1106-1124.

Funken, S., Praetorius, D., & Wissgott, P. (2011). Efficient implementation of adaptive P1-FEM in Matlab. *Computational Methods in Applied Mathematics Comput. Methods Appl. Math., 11*(4), 460-490.

Getreuer, P. (2006). Writing fast matlab code: June.

Jayaswal, K., & Grosse, I. (1993). Finite element error estimation for crack tip singular elements. *Finite elements in analysis and design, 14*(1), 17-35.

Johnson, C., & Hansbo, P. (1992). Adaptive finite element methods in computational mechanics. *Computer Methods in Applied Mechanics and Engineering, 101*(1-3), 143-181.

Li, Y., Li, M., & Liu, G. (2014). A modified triangulation algorithm tailored for the smoothed finite element method (S-FEM). *International Journal of Computational Methods, 11*(01), 1350069.

Li, Y., Liu, G., & Zhang, G. (2011). An adaptive NS/ES-FEM approach for 2D contact problems using triangular elements. *Finite elements in analysis and design, 47*(3), 256-275.

Liu, G.-R. (2009). *Meshfree methods: moving beyond the finite element method*: CRC press.

Liu, G.-R., & Gu, Y. (2001). A point interpolation method for two‐dimensional solids. *International Journal for Numerical Methods in Engineering, 50*(4), 937-951.

Liu, G. (2008). A generalized gradient smoothing technique and the smoothed bilinear form for Galerkin formulation of a wide class of computational methods. *International Journal of Computational Methods, 5*(02), 199-236.

Liu, G., Dai, K., & Nguyen, T. T. (2007). A smoothed finite element method for mechanics problems. *Computational Mechanics, 39*(6), 859-877.

Liu, G., Nguyen-Thoi, T., & Lam, K. (2009). An edge-based smoothed finite element method (ES-FEM) for static, free and forced vibration analyses of solids. *Journal of Sound and Vibration, 320*(4-5), 1100-1130.

Liu, G., Nourbakhshnia, N., Chen, L., & Zhang, Y. (2010). A novel general formulation for singular stress field using the ES-FEM method for the analysis of mixed-mode cracks. *International Journal of Computational Methods, 7*(01), 191-214.

Liu, G., Nourbakhshnia, N., & Zhang, Y. (2011). A novel singular ES-FEM method for simulating singular stress fields near the crack tips for linear fracture problems. *Engineering fracture mechanics, 78*(6), 863-876.

Lo, D. S. (2014). *Finite element mesh generation*: CRC Press.

Nguyen-Xuan, H., Liu, G., Bordas, S., Natarajan, S., & Rabczuk, T. (2013). An adaptive singular ES-FEM for mechanics problems with singular field of arbitrary order. *Computer Methods in Applied Mechanics and Engineering, 253*, 252-273.

Nguyen-Xuan, H., Rabczuk, T., Nguyen-Thanh, N., Nguyen-Thoi, T., & Bordas, S. (2010). A node-based smoothed finite element method with stabilized discrete shear gap technique for analysis of Reissner–Mindlin plates. *Computational Mechanics, 46*(5), 679-701.

Nguyen-Xuan, H., Tran, L. V., Nguyen-Thoi, T., & Vu-Do, H. (2011). Analysis of functionally graded plates using an edge-based smoothed finite element method. *Composite Structures, 93*(11), 3019-3039.

Nguyen-Thoi, T., Liu, G., Nguyen-Xuan, H., & Nguyen-Tran, C. (2011). Adaptive analysis using the node-based smoothed finite element method (NS-FEM). *International Journal for Numerical Methods in Biomedical Engineering, 27*(2), 198-218.

Niu, R., Liu, G., & Yue, J. (2018). Development of a software package of smoothed finite element method (S-FEM) for solid mechanics problems. *International Journal of Computational Methods*, 1845004.

Nourbakhshnia, N., & Liu, G. (2011). A quasi‑static crack growth simulation based on the singular ES‑FEM. *International Journal for Numerical Methods in Engineering, 88*(5), 473-492.

Rahman, T., & Valdman, J. (2013). Fast MATLAB assembly of FEM matrices in 2D and 3D: Nodal elements. *Applied mathematics and computation, 219*(13), 7151-7158.

Rivara, M.-C., & Iribarren, G. (1996). The 4-triangles longest-side partition of triangles and linear refinement algorithms. *Mathematics of Computation of the American Mathematical Society, 65*(216), 1485-1502.

Rivara, M. C. (1984). Algorithms for refining triangular grids suitable for adaptive and multigrid techniques. *International Journal for Numerical Methods in Engineering, 20*(4), 745-756.

Rosenberg, I. G., & Stenger, F. (1975). A lower bound on the angles of triangles constructed by bisecting the longest side. *Mathematics of Computation, 29*(130), 390-395.

Seweryn, A., & Molski, K. (1996). Elastic stress singularities and corresponding generalized stress intensity factors for angular corners under various boundary conditions. *Engineering fracture mechanics, 55*(4), 529-556.

Suárez, J., Plaza, A., & Carey, G. (2008). Propagation of longest‑edge mesh patterns in local adaptive refinement. *Communications in Numerical Methods in Engineering, 24*(7), 543-553.

Szabó, B., Szabo, B. A., & Babuška, I. (1991). *Finite element analysis*: John Wiley & Sons.

Tangaramvong, S., & Tin-Loi, F. (2012). An FE-MPEC approach for limit load evaluation in the presence of contact and displacement constraints. *International journal of solids and structures, 49*(13), 1753-1763.

Tangaramvong, S., Tin‑Loi, F., & Song, C. (2012). A direct complementarity approach for the elastoplastic analysis of plane stress and plane strain structures. *International Journal for Numerical Methods in Engineering, 90*(7), 838-866.

Theme, I. (1999). *A2. Imminent failure flood for a concrete gravity dam.* Paper presented at the 5th International Benchmark Workshop on Numerical Analysis of Dams, Denver.

Verfürth, R. (1994). A posteriori error estimation and adaptive mesh-refinement techniques. *Journal of computational and applied mathematics, 50*(1-3), 67-83.

Vu-Bac, N., Nguyen-Xuan, H., Chen, L., Lee, C.-K., Zi, G., Zhuang, X., . . . Rabczuk, T. (2013). A phantom-node method with edge-based strain smoothing for linear elastic fracture mechanics. *Journal of Applied Mathematics, 2013*.

Williams, M. (1952). Stress singularities resulting from various boundary conditions in angular corners of plates in extension. *Journal of applied mechanics, 19*(4), 526-528.

Zhang, Z.-Q., & Liu, G. (2010). Temporal stabilization of the node-based smoothed finite element method and solution bound of linear elastostatics and vibration problems. *Computational Mechanics, 46*(2), 229-246.

Zhong, H., Li, H., Ooi, E. T., & Song, C. (2018). Hydraulic fracture at the dam-foundation interface using the scaled boundary finite element method coupled with the cohesive crack model. *Engineering Analysis with Boundary Elements, 88*, 41-53.

Zienkiewicz, O., & Zhu, J. (1989). Error estimates and adaptive refinement for plate bending problems. *International Journal for Numerical Methods in Engineering, 28*(12), 2839-2853.

Zienkiewicz, O. C., Taylor, R. L., Nithiarasu, P., & Zhu, J. (1977). *The finite element method* (Vol. 3): McGraw-hill London.

Zienkiewicz, O. C., Taylor, R. L., Taylor, R. L., & Taylor, R. (2000). *The finite element method: solid mechanics* (Vol. 2): Butterworth-heinemann.

Zienkiewicz, O. C., & Zhu, J. Z. (1987). A simple error estimator and adaptive procedure for practical engineerng analysis. *International Journal for Numerical Methods in Engineering, 24*(2), 337-357.

VITA

NAME	Vu Hoang Le
DATE OF BIRTH	11 July 1993
PLACE OF BIRTH	Tuy Hoa city, Vietnam
INSTITUTIONS ATTENDED	Department of Civil Engineering, Faculty of Engineering, Chulalongkorn University
	Faculty of Civil Engineering, Ho Chi Minh University of Architecture
HOME ADDRESS	Room 316, Diana Court Apartment, Soi 6 Phetchaburi, Ratchathewi, Bangkok, Thailand
PUBLICATION	(1) Vu, L.H., et al., Load Rating and Buckling of Circular Concrete-Filled Steel Tube (CFST): Simulation and Experiment. IOP Conference Series: Materials Science and Engineering, 2018. 371(1): p. 012032.
	(2) "The process for designing steel connections using American Standards AISC 360-10", The Proceedings of University Conference on undergraduate research, Ho Chi Minh University of Architecture 2018.
	(3) Vu L. H., S. Tangaramvong "The Performance of 3-node Enhanced ES-FEM with Automatic Mesh Adaptation in Engineering Mechanics Applications" The 10th International Conference on Computational Methods (ICCM2019), Singapore.
	(4) Vu L. H., S. Tangaramvong "An Automatic Adaptive ES-FEM Method Applied to Mechanics Problems" The 24th

	National Convention on Civil Engineering (NCCE24), Thailand
AWARD RECEIVED	(1) Fully ASEAN Scholarship for Master degree from Chulalongkorn University
	(2) Incentive prize in National Excellent Student Contest of Physics in 2011
	(3) Two Incentive prizes in National Olympic Contest on Mechanics in 2013 and 2014
	(4) Lawrence S.Ting Scholarship provided by "Lawrence S.Ting Fund" in 2013-2014 and 2015-2016 school years.

จุฬาลงกรณ์มหาวิทยาลัย

CHULALONGKORN UNIVERSITY